


5-2017

On the Origin of Sensory Errors

Jonathan R. Flynn

Follow this and additional works at: http://digitalcommons.library.tmc.edu/utgsbs_dissertations

 Part of the [Behavioral Neurobiology Commons](#), [Cognitive Neuroscience Commons](#), [Computational Neuroscience Commons](#), [Medicine and Health Sciences Commons](#), and the [Systems Neuroscience Commons](#)

Recommended Citation

Flynn, Jonathan R., "On the Origin of Sensory Errors" (2017). *UT GSBS Dissertations and Theses (Open Access)*. 760.
http://digitalcommons.library.tmc.edu/utgsbs_dissertations/760

This Dissertation (PhD) is brought to you for free and open access by the Graduate School of Biomedical Sciences at DigitalCommons@TMC. It has been accepted for inclusion in UT GSBS Dissertations and Theses (Open Access) by an authorized administrator of DigitalCommons@TMC. For more information, please contact laurel.sanders@library.tmc.edu.

ON THE ORIGIN OF SENSORY ERRORS

by

Jonathan Richard Flynn, B.S., B.A.

APPROVED:

Harel Shouval, Ph.D.
Advisory Professor

Valentin Dragoi, Ph.D.

Giridhar Kalamangalam, Ph.D.

Keri Smith, Ph.D.

Anthony Wright, Ph.D.

APPROVED:

Dean, The University of Texas
MD Anderson Cancer Center UTHHealth Graduate School of Biomedical Sciences

ON THE ORIGIN OF SENSORY ERRORS

A DISSERTATION

Presented to the Faculty of The University of Texas Health Science Center at Houston and The
University of Texas M.D. Anderson Cancer Center

Graduate School of Biomedical Sciences

In Partial Fulfillment

of the Requirements

for the Degree of

DOCTOR OF PHILOSOPHY

by

Jonathan Flynn, B.S., B.A., Houston, Texas

January, 2017

Acknowledgements

I would first like to thank my advisor, Harel Shouval, who has given me the freedom and support to pursue projects as I see fit. I also would like to thank my lab mate and friend, Marco Huertas, who was always there to bounce ideas off of, and to point out the rare flaws in my logic.

To my advisory, supervisory, and examining committee, I would also extend my thanks. Your constructive feedback has kept me on track, and given me the insight to pursue avenues of research that I would not have thought of on my own.

To the faculty of the UTH Neuroscience, Biology and Anatomy program, thank you for building a culture that has been a pleasure to work in. In particular, I would like to thank Dr. Tony Wright for his tutelage on all matters psychophysical. Without him, the project in this dissertation could not have been completed. I would also like to thank Dr. Daniel Felleman, who provided material resources and advice on this project.

I would like to thank my many friends in Houston, who have celebrated and commiserated with me during the many ups and downs of graduate school.

Finally, I would like to state my eternal gratitude to my parents. Words cannot suffice to express how thankful I am for their love and support.

ON THE ORIGIN OF SENSORY ERRORS

Jonathan Richard Flynn, B.S, B.A

Advisory Professor: Harel Shouval, Ph.D.

Estimation of perceptual variables is imprecise and prone to errors. Although the properties of these perceptual errors are well characterized, the physiological basis for these errors is unknown. One previously proposed explanation for these errors is the trial-by-trial variability of the responses of sensory neurons that encode the percept. Initially, it would seem that a complicated electrophysiological experiment would need to be performed to test this hypothesis. However, using a strong theoretical framework, I demonstrate that it is possible to determine statistical characteristics of the physiological mechanism responsible for perceptual errors solely from a behavioral experiment. The basis for this theoretical framework is that different stochastic distributions (e.g., Poisson, Gaussian, etc.) will behave differently under temporal constraints. The results of this model connect easily with existing psychophysical techniques; additionally, I extend the theory here and show that it can generate realistic tuning curves that can predict perceptual acuity as a function of stimulus magnitude and duration. Following the analytical work, I performed the necessary experiments to test the model. I demonstrate that the physiological basis of perceptual error has a constant level of noise (i.e., independent of stimulus intensity and duration). By comparing these results to previous physiological measurements, I show that perceptual errors cannot be due to the variability during the encoding stage. Further, I show a very close fit between the theoretically generated tuning curve and the behavioral results, which gives more insight into the error

generation mechanism. Finally, I find that the time window over which perceptual evidence is integrated lasts no more than ~230ms. I discuss these results and others, and speculate on sources of error that may be consistent with my behavioral measurements.

Table of Contents

Acknowledgements.....	iii
Abstract.....	iv
Table of Contents.....	vi
List of Figures	viii
List of Tables.....	ix
1.1 – Chapter 1: Introduction.....	2
2.1 – Introduction.....	14
2.2 – Mathematical methods and results.....	16
2.2.1 - Model assumptions and overview	16
2.2.2 - Derivation of Equation 2.1 and 2.2.....	20
2.2.3 - The implications of variable firing rates	25
2.2.4 - The impact of errors in estimating temporal intervals	27
2.2.5 – Fitting stimulus magnitude and duration.....	31
2.2.5.1 – Analytical work	32
2.2.5.2 - Monte Carlo verification	34
2.3 – Conclusions.....	39
2.3.1 – Neuronal noise as a source of perceptual error	39
2.3.2 – Errors in timing as a source of perceptual error	40
2.3.3 – Predicting JND as a function of stimulus magnitude and duration.....	40
3.1 – Introduction.....	43
3.2 - Methods	44
3.2.1 - Experimental Design	44
3.2.1.1 - Hardware Setup	47
3.2.1.2 - Training	47
3.2.1.3 - Stimuli.....	48
3.2.2 – Adaptive Algorithm.....	50
3.2.2.1 - Bayesian adaption algorithm alterations and set up	51
3.2.2.2 – Convergence and exclusion criteria.....	52
3.2.2.2 - JND Value.....	53
3.2.2.4 – Proof of convergence through Monte Carlo simulation	53
3.2.3 - Calculating JND Related Measures	57
3.3 - Results	59

3.3.1 - Primary results	59
3.3.2 – Testing with respect to scalar timing	62
3.3.3 – Bias and order preference	63
3.3.4 – Fitting stimulus magnitude and duration.....	67
3.4 - Conclusion.....	75
3.4.1 - Behavioral noise.....	75
3.4.2 - Integration Window	77
Chapter 4 - Conclusion.....	80
Bibliography	87
Vita.....	91

List of Figures

Figure 1.1: Two stereotypical psychometric curves.....	4
Figure 1.2: Examples of noise paradigms	8
Figure 2.1: Theoretical foundation.....	18
Figure 2.2: Demonstration of the effect of timing estimation errors	31
Figure 2.3: Applying gradient descent to build a tuning curve	35
Figure 2.4: Simulation of psychophysical task using the derived tuning curve	37
Figure 3.1: Experimental Methods	46
Figure 3.2: Alterations from Kontsevich and Tyler (1999)	51
Figure 3.3: A Monte Carlo simulation of the adaptive algorithm.....	56
Figure 3.4: Individual and combined Log-JND-Ratio plots	59
Figure 3.5: ρ and τ_{sat} values across reference contrast conditions.....	62
Figure 3.6: Establishing α	68
Figure 3.7: Determining ϕ	70
Figure 3.8: Two parameter fitting of the behavioral data	71

List of Tables

Table 2.1: Condition descriptions.....	38
Table 2.2: Comparing Monte Carlo and analytical results.....	38
Table 3.1: Summarized data from each subject.....	61
Table 3.2: Measurements of bias.....	64
Table 3.3: JND results across different conditions.....	66
Table 3.4: Numerical results for Weber correction in different time conditions.....	69
Table 3.5: Comparing experimental results to model predictions.....	73

CHAPTER 1: INTRODUCTION

1.1 – Introduction

When we perceive the world, there is naturally some level of error. A musician tuning their instrument may occasionally be off on their pitch. When trying to catch a ball, a baseball player might misjudge where it is. After sitting in a dark movie theater, we often miscalculate the length of a film. In short, our perception does not completely match the truth of the external world. However, the types of errors that are made are often systematic; specific patterns have been found across different sensory mechanisms, suggesting a common source for our misperceptions (Coren et al., 2003; Kandel et al., 2012). Here, we use a combination of theoretical and experimental work to figure out the source of sensory errors.

1.1.1 – Psychophysics and its physiological basis

The study of sensory errors has a long pedigree. One of the earliest scientific forays into studying the mind was the field of *psychophysics*, which is a continuing attempt to mathematically link physical stimuli with mental phenomenon. The first experiments in the field were simple: subjects were asked to compare two weights and determine whether they were the same or different (Fechner, 1860; Weber, 1834). An intuitive but important conclusion was reached: the change in weight required for a subject to just notice a difference scaled linearly with the magnitude of the original weight. To put it more concretely, if a 10-gram weight required 1-gram change for a subject to notice a difference, a 100-gram weight would require a 10-gram change for the same subject to notice a difference. This linear relationship is called the Weber-Fechner Law, and is one of the most fundamental observations in psychophysics.

Over the past 150 years, the field of psychophysics has codified methods of talking about perceptual errors. The most common measurement is the Just-Noticeable-Difference, or JND, and is found by establishing a psychometric curve (Klein, 2001). The psychometric curve is a sigmoid function that describes a subject's error rate in either discriminating or detecting a stimulus (See Figure 1.1). In the test to establish this function, two stimuli are presented: a reference and a test. Depending on the nature of the experiment, these stimuli might be presented serially or concurrently. Regardless, the subject is asked whether the test stimulus has a higher magnitude than the reference stimulus. The probability of answering 'yes' is ascertained by repeating for many trials, and the magnitude of the test stimulus is varied to build the entirety of the psychometric function. The JND is established by finding a stimulus magnitude that corresponds to an arbitrary percentage correct (often 75%, although here we will use 84% for reasons described later), and subtracting the reference magnitude. Assuming no bias in subject response (i.e., the subject chooses randomly when uncertain), this is an easily communicated proxy for the slope of the psychometric function. Multitudes of variations on this paradigm exist (Klein, 2001), and are discussed further in Section 3.2.2, along with their ramifications on the work presented here.

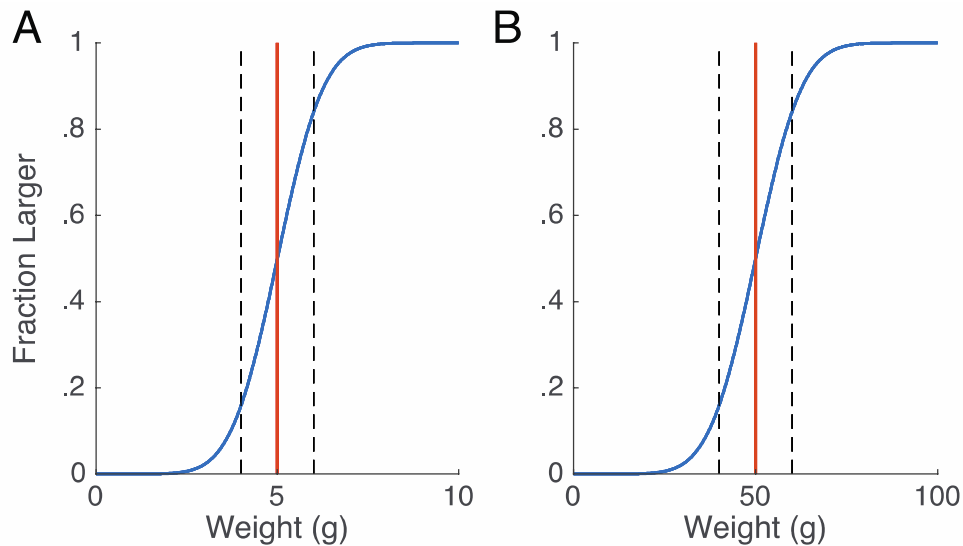


Figure 1.1: Two stereotypical psychometric curves

Above we see two cartoon psychometric curves. The red line corresponds to the magnitude of the reference stimuli, while the dashed lines represent the Just-Noticeable-Difference (JND). The X-axis represents the magnitude of the test stimuli. The probability of that test stimuli being perceived as higher is demonstrated on the Y-Axis. Note that the different graphs have different stimuli (**A** – 5 grams; **B** – 50 grams), but the psychometric function linearly scales to fit the increase. The current graph denotes weight, but the psychometric function is used in every sensory modality.

Using this methodology, or similar ones, the statistical properties of perceptual estimation errors are rigorously studied (Coren et al., 2003; Ehrenstein and Ehrenstein, 1999; Kandel et al., 2012). Experiments have shown that the above-mentioned Weber-Fechner Law, or a fair approximation of it, applies to nearly every sensory modality. For example: brightness and loudness (Fechner, 1860), color (Indow and Stevens, 1966), loudness (where it is a near miss) (McGill and Goldberg, 1968), touch/vibration sensitivity (Gescheider et al., 1990), timing (Gibbon, 1977) and even abstract concepts like numerosity (Nieder and Miller, 2003). Because this pattern is so pervasive, it suggests

that there may be a common physiological mechanism that is generating the same type of error.

One belief in the field, often tacit but sometimes stated outright (Tolhurst et al., 1981), is that neural variability gives rise to observed psychophysical phenomenon. This has intuitive appeal – it is well established that neurons, *in vivo*, have stochastic properties (Stein et al., 2005). Repeated trials of identical stimuli show variability in the number of spikes elicited, most often with variances proportional to the mean (Heggelund and Albus, 1978; Tolhurst et al., 1983). It is likely that much of this variability is innate to the neurons, due to balances of inhibition and excitations (Hertz et al., 2003; van Vreeswijk and Sompolinsky, 1996). The statistical properties of trial-by-trial spike variability have been well studied (Churchland and Abbott, 2012; Dean, 1981a; Mainen and Sejnowski, 1995), and it seems natural that variability in the processing of information will lead to variability in sensory judgement. Previous theoretical research has assumed trial-by-trial spike rate variability as a source for behavioral variability in psychophysical tasks (Goris et al., 2009; May and Solomon, 2015a, 2015b; Mazurek et al., 2003; Shouval et al., 2013). Further, electrophysiological experiments have related trial by trial variability of sensory neurons to behavior (Britten et al., 1993, 1996; Cohen and Newsome, 2009; Shadlen et al., 1996). However, it is important to note that other interpretations of behavioral variability exist. For example, it has been suggested that uncertainty about the meta-information of the signal (e.g., its size, position in the visual field, time of presentation start and the duration, etc.) may account for much of the behavioral variability we see (Pelli, 1985). I will discuss these theories, and the ramifications of the current work on them, further in Chapter 4.

1.1.2 – Connecting physiology to behavior

The goal of the current work is to test whether trial-by-trial variability in spike rate can account for the behavioral errors quantified in psychophysical experiments. On the surface, a large scale electrophysiological experiment would seem to be required to resolve this question. However, with theory I can show a necessary relationship between neuronal spiking statistics and behavior. The present project is broken up into two sub-aims:

- 1) To develop a mathematical formalism from first principles that connects neuronal variability with measurable rates of behavioral errors. (Chapter 2)
- 2) To develop a behavioral experiment on the principles of the above formalism, and determine whether trial-by-trial variability in neuronal spiking can account for the perceptual errors. (Chapter 3)

To set up the theoretical foundations for the current experiment, we first need to understand that the statistics of the encoding neuron set the lower limit of behavioral noise (Paradiso, 1988; Seung and Sompolinsky, 1993). Using Fisher information, we can quantify the amount of information a stochastic spike train has encoded about a given stimulus. Based on the characteristics of the firing rate variability, when this information is decoded (i.e., it is interpreted for use in a behavioral decision), there will necessarily be some loss of the original information. This loss can also be quantified, and from that, there is a minimum level of error that is tautologically accounted for by neuronal stochasticity.

In other words, using basic information theory, we can say that the trial-by-trial variability will necessarily add a certain amount and type of error to perception. If perceptual errors differ from this prediction, it suggests that neuronal variability is not the source (or at least the sole source) of perceptual errors. This analytical work for this theory is further developed in Section 2.2.

It is important to note that all the theoretical work in this dissertation is built on 3 simple assumptions:

- 1) Perceptual judgements are based on the number of spikes in a given time window.
- 2) The tuning curve is monotonic (i.e., when the stimulus magnitude increases, the average firing rate increases)
- 3) The variability of the spike count in a given time window can be approximated by a power law.

To give an intuition on what these mean, we can return to the example of weight given above. If we were to measure a neural response to a weight stimuli, we could imagine a tuning curve ($r(\theta)$) like the one presented in Figure 1.2 (black-dashed line). In general, when the subject is given a 30-gram weight, the firing rate will higher than if the subject were given a 15-gram weight. Areas of the brain that are responsible for deciding on which weight is heavier would determine this by ‘counting’ the number of spikes in a certain time window and calculating the spike rate. In general, this calculation will

determine that the spike rate for the 30-gram weight is higher than for the 15-gram weight (and therefore that the 30-gram weight is heavier than the 15-gram weight). However, due to spike count stochasticity, the opposite should occasionally occur.

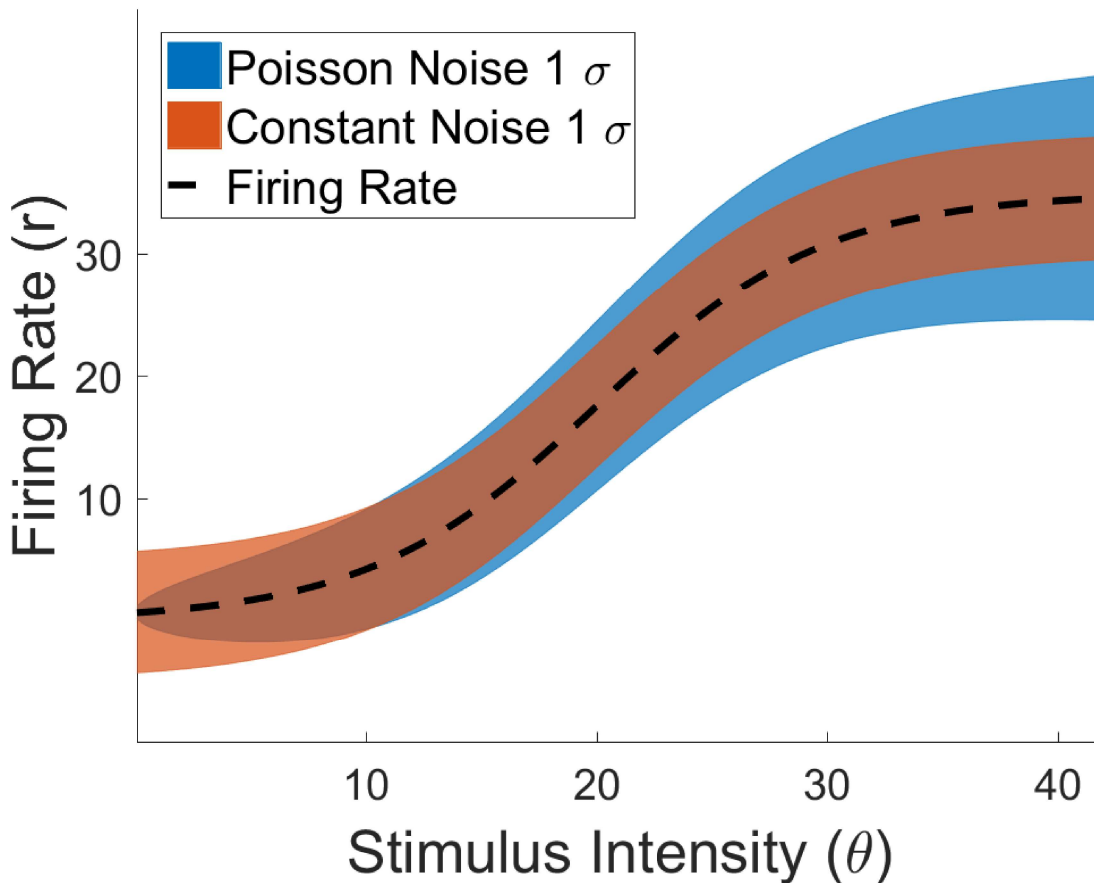


Figure 1.2: Examples of noise paradigms

The above figure demonstrates the impact of noise characteristics on the firing rate. For the same tuning curve (black dashed line), we will see different results. The blue denotes the 1σ distribution for a Poisson spiking neuron, while the orange denotes the 1σ distribution for a neuron with a constant noise. Notes the differences between the two, particularly at the two extremes of stimulus intensity.

To understand the ramifications of these assumptions, we must first discuss the nature of neuronal noise. Neurons with *constant noise* would have the same variance, regardless

of the stimulus intensity/firing rate. Neurons with *Poisson noise* would have a variance proportional to the stimulus intensity/firing rate. Figure 1.2 graphically presents a cartoon example of this. In general, neurons tend to have Poisson variability (Dean, 1981a), although exceptions exist (Zhong et al., 2005). The innovation presented in this paper is that different types of variability exist (e.g., Poisson, Constant – blue and orange respectively in Figure 1.2), and these will have measurable impacts on behavior. By approximating this variability with a power law (Assumption 3), we can analytically derive a probabilistic spike count distribution for a given time window (Assumption 1). These spike count distributions can be either for a single neuron or for a group of neurons – it is immaterial to the model at hand. Once the spike count distributions are generated, we can compare what happens when two different magnitudes of stimuli are presented – where these curves overlap, a perceptual mistake will be made (further description in Chapter 2). This overlap corresponds to the JND in the traditional psychometric function, and it is this correspondence that allows me to build an experiment to test the current model (Chapter 3).

What is notable about this model is that it makes a singular prediction. Intuitively, as we decrease the amount of time to perceive a stimulus, the perceptual error rate will go up. What I will show in Chapter 2 is that truncating the time window of perception is more deleterious to discrimination ability in the constant noise scenario than in the Poisson noise scenario. Further, the current model makes very specific predictions on the ratio of the JNDs at two different time points, allowing us to determine definitively which noise distribution is responsible for causing perceptual errors. The analytical calculation that

underpin these claims have been verified with computational simulations. The result of this theoretical work is that it is now possible to make claims about the statistical nature of the physiology generating perceptual errors solely from a behavioral experiment. This, in turn, allows for the elimination of certain well described physiological systems as the source of perceptual error.

1.1.3 – Testing the model

Since the model described above makes predictions about the ratios of JNDs at different times, I designed an experiment to specifically test those predictions. A further requirement was that I needed to know the spiking statistics of the sensory modality being tested. Contrast detection neurons are well characterized as possessing a monotonic tuning curve (Dean, 1981b) and having a Poisson-like variability (Dean, 1981a), so I chose to have contrast grating be my sensory stimulus.

Overall, I recruited 9 visually normal (or corrected to normal) subjects, with ages ranging from 20-45. Two were rejected for poor performance during the task. Subjects were placed in a darkened room and instructed to use a chin rest to make sure that they would not change perspectives during the experiment. Once the experiment was initiated, subjects were presented with stationary gratings with a randomized phase and a spatial frequency of 1 cycle/degree of vision. Subjects were asked to discriminate between two gratings (a reference and a test) and to report which one they perceived as having a higher contrast. Visual masks were used to 1) reduce the effects of afterimages, and 2) maintain subjects in the same contrast adaptations (Heinrich and Bach, 2001). For

conditions in this experiment, I manipulated the presentation time of both gratings (ranging from 50 to 600 ms) as well as the intensity of the reference stimuli.

To find the JND for each condition combination using traditional psychometric techniques, I would have had to collect upwards of 30,000 trials per subject. This is equivalent to over 50 days of experiment time per subject (at 1 hour per day), which was infeasible. However, I was able to modify and apply an adaptive algorithm (Kontsevich and Tyler, 1999) to the experimental methodology, reducing the number of samples needed to approximately 7,000 per subject. In practice, the algorithm gave more difficult test stimuli (i.e., closer in magnitude to the reference stimuli) when subjects were performing well. When subjects performed poorly, they were given easier test stimuli. Details on the mathematics behind this, as well as other experiment features, can be found in Section 3.2.

The first thing that I found was that there is a limited integration window for contrast stimuli. After ~230 ms, subjects gain no additional discrimination ability for longer stimulus presentation times. This is somewhat consistent with existing literature on the subject, which report approximately 100 ms integration windows, with a large variability depending on the spatial frequency (Legge, 1978). However, the data here represents a far more precise measure, given the number of samples and the optimization effects of the Bayesian algorithm. In Section 3.4.2, I discuss the ramifications of this result, and suggest how it can be related to other physiological phenomena, such as neuronal spiking dynamics (Heller et al., 1995) and intersaccade intervals (Carpenter, 1988).

More importantly, I also show that trial-by-trial variability in neuronal spiking *cannot* account for perceptual errors. While contrast processing neurons in the V1 have a Poisson spiking pattern (Dean, 1981a), the current behavioral data suggests that whatever generates the behavioral variability must have a constant noise. This demonstrates that, rather than errors occurring during encoding, errors must propagate from the decoding process. In Section 3.4.1, I discuss how to reconcile a constant level of behavioral noise with the existing literature. This is followed by a discussion in Section 4 on the possible components of the decoding process that could generate a constant noise, and speculation on how to differentiate between those components experimentally.

Chapter 2: Formalizing the connection between trial-by-trial variability and perceptual errors

2.1 – Introduction

In order to interact with the world, all animals must estimate the magnitude of external stimuli; it is well established that this process is prone to errors (Coren et al., 2003; Dayan and Abbott, 2005; Kandel et al., 2012). These errors form the foundation of the science of psychophysics, and have been studied as far back as the 19th century (Weber, 1834). However, while the statistical properties of these estimation errors have been rigorously studied in multiple sensory systems (Coren et al., 2003; Kandel et al., 2012), their physiological source is unknown.

One possible physiological source of perceptual errors is the variability of sensory encoding neurons. When the same sensory percept is presented repeatedly, the number of action potentials generated by a sensory neuron varies from trial-to trial (Stein et al., 2005). Characterizing the statistical properties of spike rate variability has been an active field of study (Churchland et al., 2010; Dean, 1981a; Mainen and Sejnowski, 1995). Theoretical examinations have previously assumed that such variability in sensory neuron responses contribute to behavioral variability (May and Solomon, 2015a, 2015b; Mazurek et al., 2003; Shouval et al., 2013). Moreover, several experiments that have related the trial-by-trial variability of sensory neurons to behavior (Britten et al., 1993, 1996; Cohen and Newsome, 2009; Shadlen et al., 1996) seem to bolster the hypothesis that the trial-by-trial variability of sensory neurons is the origin of behavioral variability, though alternative interpretations are possible.

Previous experiments that have tested the relationship between neural firing rate variability and behavior have required extensive electrophysiological setups (Britten et al., 1993, 1996; Shadlen et al., 1996). Here, I demonstrate analytically that it is possible to gain significant insight into the physiology generating perceptual errors solely from psychophysical experiments. Using the inverse of the Fisher information (a typical measurement of the amount of information in a spike train), there is necessarily a lower limit of perceptual errors that are caused by spike rate variability (Paradiso, 1988; Seung and Sompolinsky, 1993). To give an intuitive example, a theoretical neuron that could be relied upon to generate a spike rate of 50 ± 1 Hz with a 20 Lumen stimulus can be mathematically shown to be able to encode more information than one that would spike at 50 ± 10 Hz for the same stimuli. As the variability of the encoding function increases, the information that can be transmitted to the next stage of sensory processing decreases. However, in real neural systems, variability is often dependent on firing rate (Dean, 1981a). Thus, the lower limit of perception is defined by the statistical properties of the sensory encoding neurons, such as whether the firing rate variability is constant or Poisson. The central insight of this dissertation is that, by changing the integration time of a spike train, we can show quantifiably different effects on perceptual accuracy for different neuronal variability condition. Thus, we can develop an experiment that can infer key statistical properties of the neural noise that generates perceptual errors simply by altering the viewing time of a stimuli. The current chapter focuses on the analytical framework of this theory. Chapter 3 describes the experimental implementation of this theory, and interprets that implementation's results.

2.2 – Mathematical methods and results

2.2.1 - Model assumptions and overview

Intuitively, if we decrease the amount of time that a person has to perceive a stimulus, there will be some level of corresponding decrease in the person's perceptual precision. Here, I outline a theoretical framework from which one can determine key statistical properties of the noise that drives perceptual errors by measuring this change in sensory discrimination ability. This theoretical framework is based on the three following assumptions:

1. Perceptual judgment is obtained based on the number of spikes in a time window of length τ (Figure 1A).
2. The spike-count tuning curve, $R(\theta, \tau)$, is monotonic, where θ is the perceptual variable; note that this tuning curve could describe either single neurons, or a combined variable due to a population of neurons.
3. The variability in the spike count (σ) can be approximated by $\sigma = \beta \cdot R(\theta, \tau)^\rho$, where β and ρ are empirically determined constants (Dean, 1981). For example, a value of $\rho = 0.5$ would represent a Poisson-like relationship between firing rate and noise, whereas a value of $\rho = 0$ would represent a constant noise level, independent of the firing rate.

We also incorporate the additional assumption that for any given stimuli, there is a time (τ_{sat}) such that for observation times $\tau > \tau_{sat}$, performance at sensory discrimination will not improve. This assumption is motivated by my experimental data, which exhibit

performance saturation as a robust phenomenon. However, were my data sets not to include time points beyond τ_{sat} , the current theory would still be able to determine ρ .

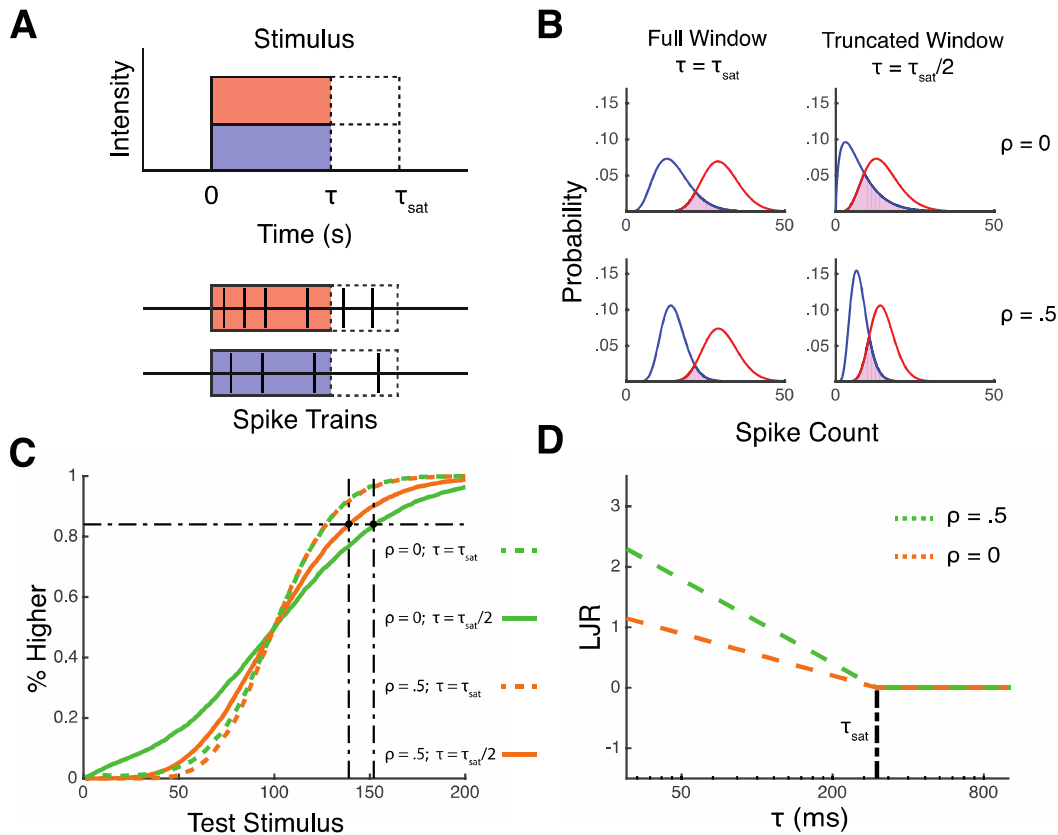


Figure 2.1: Theoretical foundation

A: Neural responses vary depending on the intensity of a stimulus. For the same τ , a low magnitude stimulus (blue) will, on average, generate fewer spikes than a high magnitude stimulus (red). If the presentation time of the stimulus is truncated ($\tau < \tau_{sat}$; dashed regions), fewer spikes will be counted on average. **B:** Spike count distributions for different ρ and τ conditions are represented here (arbitrarily) using gamma distribution functions. The size of the magenta region (i.e., the overlap coefficient) is directly related to discrimination ability. **C:** From the overlap coefficients, we can calculate psychometric curves, and thus JND_{τ} , for different conditions. Note how changes in τ affect the ρ conditions differently. **D:** Behavioral values of JND_{τ} cannot be derived axiomatically. However, using Equation 2, we can predict the ratio between JND_{τ} and JND_{sat} . Note when $\tau \geq \tau_{sat}$, $LJR = 0$.

From these assumptions, we can derive a relationship between the variability in stimulus estimation and the spiking statistics. I start by relating the behavioral estimation error to the statistics of the encoding signal, using the equation:

$$(2.1) \quad \sigma_{\theta}^2 = \frac{\sigma_R^2}{(R')^2}$$

where σ_{θ} is the standard deviation of the stimulus estimation, σ_R is the standard deviation of the encoding variable $R(\theta, \tau)$, and R' is the derivative of R with respect to θ . Note that $R(\theta, \tau)$ is a tuning curve in terms of spike count, and depends both on the encoded parameters θ , and on the duration of the stimulus presentation τ . R can be either a single neuron-tuning curve or a population coding based tuning curve. Equation 2.1 is, for many forms of encoding statistics, a close approximation of the inverse Fisher information (Paradiso, 1988; Seung and Sompolinsky, 1993). Therefore, it estimates the perceptual error given an optimal decoding strategy from the spike count. A more detailed derivation is presented in Section 2.2.2 in this chapter.

The ability to distinguish two stimuli depends on the spike count distributions arising from these stimuli, characterized by R and σ . The overlap between the distributions (Figure 1B, magenta regions) determines the probability that the subject will mistakenly believe that the lower magnitude stimulus is the higher one. This overlap is related to the traditional Just-Noticeable-Difference (*JND*) psychometric function (Figure 1C – see (Klein, 2001) for further background). As τ is reduced, the spike count is reduced, the distributions are altered (Figure 1B), and the overlap region (and thus *JND*) increases. The increase in the overlap depends both on the change in the mean spike count and on

the variance of the spike count. Therefore, for different statistical models of noise, the change in overlap will be quantifiably different. In this particular example, we observe that decreasing τ has a more deleterious effect on discrimination ability in the $\rho = 0$ case than in the $\rho = 0.5$ case (Figure 1C). The relationship between τ and the JND can be mathematically formalized (see Section 2.2.2) with the following equation:

$$(2.2) \quad LJR = \log\left(\frac{JND_{\tau}}{JND_{sat}}\right) = (\rho - 1) \cdot \log(\tau) - (\rho - 1) \cdot \log(\tau_{sat}); \quad \tau < \tau_{sat}$$

where LJR is the Log-JND-Ratio (defined here), JND_{τ} is the JND for a time window of length τ , and JND_{sat} is the JND for $\tau \geq \tau_{sat}$. For $\tau > \tau_{sat}$, the $LJR = 0$. By plotting LJR against $\log(\tau)$, we arrive at a line whose slope and intercept can be used to calculate ρ and τ_{sat} (see the Section 2.2.2 for derivation details). This function is plotted in Figure 1D for two specific cases: $\rho = 0$ (constant noise) and $\rho = 0.5$ (Poisson-like noise). I should note that Equation 2.2 was derived on the assumption of a constant firing rate. However, I show in Section 2.2.3 that the conclusions drawn from Equation 2.2 apply in the case of firing rates that vary over time.

2.2.2 - Derivation of Equation 2.1 and 2.2

For ease of understanding, my initial derivation will require an additional assumption from the ones listed in the main paper, namely that *the firing rate is constant and does not depend on time*. However, I will demonstrate in Section 2.2.3 how we can generalize the derivation beyond this assumption.

For many cases (e.g., Gaussian, Poisson), Equation 2.1 is exactly the inverse of the Fisher information; in other cases, it is a close approximation (Paradiso, 1988; Seung and Sompolinsky, 1993). Due to the Cramer-Rao lower bound, this sets the lower limit of the accuracy of decoding; for many distributions the optimal decoder is efficient and can attain the lower bound (Wijsman, 1973). Therefore, any significant behavioral errors more than this lower bound are decoding errors.

Here, we slightly generalize this equation to include two distinct sources of noise. One source of noise is due to variability in the spike count of the encoding neurons; the other is in the reference spike count, which is part of the decoding process.

The spike count on each trial can be used to estimate the magnitude of the stimulus on the trial. On each trial, we assume the existence of a variable T , which is used by the decoding mechanism to obtain an estimate of the variable θ . In the absence of noise, if $R(\theta) = T$, then the magnitude of variable θ could be easily determined using $\theta = R^{-1}(T)$ (note that, for convenience, we suppress the variable τ). However, both the spike-count on each trial and the reference variable can be contaminated by noise. Thus, the process can be described by:

$$(2.3) \quad R(\theta) + \Delta R = T + \Delta T$$

where ΔR is the variability in the spike count and ΔT is the variability of the reference variable. Using the same procedure to obtain an estimate of θ yields:

$$(2.4) \quad \hat{\theta} = R^{-1}(T + \Delta T - \Delta R)$$

where $\hat{\theta}$ is the stimulus magnitude estimate for a single trial. Using a first order Taylor series expansion, we come to the equation:

$$(2.5) \quad \Delta\theta = \hat{\theta} - \theta = \frac{\Delta T - \Delta R}{R'}$$

where $\Delta\theta$ is the difference between the subject's estimate of stimulus magnitude and the true value of the stimulus magnitude. By squaring both sides, and taking the average of the variances, we get:

$$(2.6) \quad \sigma_{\theta}^2 = \left(\frac{\sqrt{\sigma_R^2 + \sigma_T^2}}{R'} \right)^2$$

where σ_{θ} is the standard deviation of the magnitude estimation, σ_R is the standard deviation of the spike count, and σ_T is the standard deviation of the decision-making process. This generalization arises because the variance of two independent variables is summed. Note that, under the assumption that $\sigma_T \ll \sigma_R$, this equation is like Equation 2.1. With the assumption of a constant firing rate (r), we can convert the above equation to a function of τ :

$$(2.7) \quad \sigma_{\theta}(\tau) = \frac{\sqrt{\sigma_R^2 + \sigma_T^2}}{\tau \cdot r'}$$

where $R(\theta) = \tau \cdot r(\theta)$, and can be thought of as the spike count for a given time window, τ . Without a complicated electrophysiology experiment, we cannot know the true function $r(\theta)$. However, this function can be eliminated if we make a ratio between the standard deviations at two values of τ . Specifically, we use τ_{sat} and τ_1 , which is any $\tau < \tau_{sat}$.

$$(2.8) \quad \frac{\sigma_{\theta}(\tau_1)}{\sigma_{\theta}(\tau_{sat})} = \left(\frac{\tau_{sat}}{\tau_1} \right) \frac{\sqrt{\sigma_R^2(\tau_1) + \sigma_T^2(\tau_1)}}{\sqrt{\sigma_R^2(\tau_{sat}) + \sigma_T^2(\tau_{sat})}}$$

While we know that there is noise in the firing rate of neurons (the encoding of the stimulus), and that it is substantial, there is also possibly noise in the decoding process. The decoding process includes things like storage of information into memory (Hubbard, 1994) and the decision-making (Deco and Rolls, 2006; Deco et al., 2007), which can both introduce noise. It is possible to analyze three cases – the decoding noise is substantially less than the firing rate noise, the decoding noise is comparable to the firing rate noise, or the decoding noise is substantially larger than the firing rate noise. The latter two cases are more complicated and touched upon in the Section 3.3 and 3.4. The first case ($\sigma_T \ll \sigma_R$), however, is tractable for experimentation. We show below that it makes a strong behavioral prediction that can be tested, and it is this prediction that is central to this dissertation.

First, we will assume σ_R follows a general power law (Shouval et al., 2013):

$$(2.9) \quad \sigma_R(\theta, \tau) = \beta(\tau * r(\theta))^{\rho}$$

Combining Equations 2.8 and 2.9, and assuming ($\sigma_T \ll \sigma_R$), we can simplify to the following:

$$(2.10) \quad \frac{\sigma_{\theta}(\tau_1)}{\sigma_{\theta}(\tau_{sat})} = \frac{\tau_{sat}}{\tau_1} \frac{\beta(\tau_1 r(\theta))^{\rho}}{\beta(\tau_{sat} r(\theta))^{\rho}}$$

σ_{θ} can be considered equivalent to the behavioral measurement, *JND*. With this in mind, and canceling out β and r :

$$(2.11) \quad \frac{\sigma_{\theta}(\tau_1)}{\sigma_{\theta}(\tau_{sat})} = \frac{JND_{\tau}}{JND_{sat}} = \frac{\tau_{sat}}{\tau_1} \frac{\tau_1^{\rho}}{\tau_{sat}^{\rho}}$$

Simplifying:

$$(2.12) \quad \frac{JND_{\tau}}{JND_{sat}} = \left(\frac{\tau_1}{\tau_{sat}}\right)^{\rho-1}$$

$$(2.13) \quad \log\left(\frac{JND_{\tau}}{JND_{sat}}\right) = LJR = (\rho - 1)\log(\tau_1) - (\rho - 1)\log(\tau_{sat}) \quad \text{for } \tau \leq \tau_{sat}$$

Note that this is the same as Equation 2.2. If we plot the Log-JND-Ratio (LJR) on the y-axis, and $\log(\tau)$ on the x-axis, we will come up with the graph seen in Figure 3.1D. The slope and y-intercept can be calculated with a linear regression, and related to the values τ_{sat} and ρ with the following equations derived from Equation 2.13:

$$(2.14) \quad \begin{aligned} m &= \rho - 1 & b &= (1 - \rho)\log(\tau_{sat}) \\ \rho &= m + 1 & \tau_{sat} &= \exp\left(\frac{b}{1-\rho}\right) \end{aligned}$$

where m is the calculated slope of the line, and b is the calculated y-intercept. Thus, using a simple regression analysis on behavioral data, we can show important statistical characteristics of the sensory integration mechanism.

In dealing with the case that $\sigma_T \gg \sigma_R$, we can make an initial assumption that the decoding process has a constant level of noise, which is independent of stimulus duration or magnitude. If true, then the formulas in Equation 2.13 and 2.14 still hold, with $\rho \approx 0$.

2.2.3 - The implications of variable firing rates

To make the math simpler in the above section, I assumed that firing rate ($r(\theta)$) was a static function (i.e., the firing rate does not change over time). However, this is not a biologically realistic assumption; firing rates often have temporal dynamics. In this section, I demonstrate why this does not matter for my model.

Let us assume that the spike count function ($R(\theta)$) is separable, and can be written as a multiplication of two functions; $g(\tau)$ that accounts for the spike count for a given window τ , and $f(\theta)$ that modulates the spike count for different stimulus intensities. Thus:

$$(2.15) \quad R(\theta, \tau) = g(\tau)f(\theta)$$

We can insert the above equation into Equation 3.1, resulting in

$$(2.16) \quad \sigma(\tau) = \frac{\sigma_R}{g(\tau)f'(\theta)}$$

Following the same process we did in the previous section where we created a ratio between $\sigma_\theta(\tau_1)$ and $\sigma_\theta(\tau_{sat})$, we arrive at:

$$(2.17) \quad \frac{\sigma_\theta(\tau_1)}{\sigma_\theta(\tau_{sat})} = \frac{\sigma_R(\tau_1)}{g(\tau_1)f'(\theta)} / \frac{\sigma_R(\tau_{sat})}{g(\tau_{sat})f'(\theta)}$$

Rearranging and combining with Equation 2.9:

$$(2.18) \quad \frac{\sigma_\theta(\tau_1)}{\sigma_\theta(\tau_{sat})} = \frac{JND_\tau}{JND_{sat}} = \frac{g(\tau_{sat})}{g(\tau_1)} * \frac{\beta * g(\tau_1)^\rho f(\theta)^\rho}{\beta * g(\tau_{sat})^\rho f(\theta)^\rho}$$

$$(2.19) \quad \frac{JND_{\tau}}{JND_{sat}} = \left(\frac{g(\tau_{sat})}{g(\tau_1)} \right)^{1-\rho}$$

For presentation times over approximately 75 ms, we can assume that the firing rate is falling (See Fig 8 in Albrecht et al., 2002). This means that $g(\tau)$ is less than linear, and can be approximated with the following equation:

$$(2.20) \quad g(\tau) = \tau^{\eta} \quad \text{for } 0 < \eta < 1$$

Plugging this in to Equation 2.19:

$$(2.21) \quad \frac{JND_{\tau}}{JND_{sat}} = \left(\frac{\tau_1}{\tau_{sat}} \right)^{\eta(\rho-1)}$$

Taking the logarithm of both sides allows us to compare to Equation 2.13:

$$(2.22) \quad \log\left(\frac{JND_{\tau}}{JND_{sat}}\right) = LJR = \eta(\rho - 1) \log(\tau_1) - \eta(\rho - 1) \log(\tau_{sat}) \quad \text{for } \tau \leq \tau_{sat}$$

Just like with Equation 2.13, if we plot LJR against $\log(\tau_1)$, the slope (m) of this line will be equivalent to the coefficient of $\log(\tau_1)$.

$$(2.23) \quad m = \eta \cdot (\rho - 1)$$

It is well established that firing rates of sensory neurons tend to fall over time; a biologically plausible estimation of η would be less than one. Assuming a Poisson noise characteristic ($\rho \cong .5$), the slope of the LJR graph (Figure 1D) would be $-.5 < m < 0$. This will be tested against in Chapter 3.

2.2.4 - The impact of errors in estimating temporal intervals

Rather than a spike count variable (S), it is possible that a decision is made based on a deduced spike rate variable (r). In this section, I analyze the impact of temporal estimation errors on stimulus magnitude estimation.

By definition, $r = S/\tau$, where τ is the presentation time of the stimulus. Assume that there are two sources of noise: noise in the spike count (ΔS), and noise in the estimation of the temporal interval ($\Delta\tau$). Therefore, on each trial $S = \langle S \rangle + \Delta S$ and $\tau = \langle \tau \rangle + \Delta\tau$, where $\langle \rangle$ represents the expectation value. For simplicity, these calculations assume that $\Delta\tau \ll \tau$ and $\Delta S \ll S$. This coheres with behavioral experiments in scalar timing, which suggests that $\Delta\tau$ is approximately 10% of τ (Buhusi and Meck, 2005) and in the current experiment where ΔS is approximately 10-20% of S , although this varies particularly at low stimulus durations. We will also consider here the case where $\Delta S \ll \Delta\tau$. First, we obtain:

$$(2.24) \quad r = \frac{S}{\tau} = \frac{\langle S \rangle + \Delta S}{\langle \tau \rangle + \Delta\tau} \approx \frac{S + \Delta S}{\langle \tau \rangle} \cdot \left(1 - \frac{\Delta\tau}{\langle \tau \rangle}\right) \approx \frac{\langle S \rangle}{\langle \tau \rangle} + \frac{\Delta S}{\langle \tau \rangle} + \Delta\tau \frac{\langle S \rangle}{\langle \tau \rangle^2}$$

We will now take the square and then average r to obtain the variance of the r variable:

$$(2.25) \quad r^2 \approx \left(\frac{\langle S \rangle}{\langle \tau \rangle}\right)^2 + \Delta S \frac{\langle S \rangle}{\langle \tau \rangle^2} - \Delta\tau \frac{\langle S \rangle^2}{\langle \tau \rangle^3} - \Delta S \cdot \Delta\tau \frac{\langle S \rangle}{\langle \tau \rangle^3} + \frac{\Delta S^2}{\langle \tau \rangle^2} + \Delta\tau^2 \frac{\langle S \rangle^2}{\tau^4}$$

We now take the average. Note that any term linear with respect to $\Delta\tau$ or ΔS must vanish. Additionally, if the distribution of τ is independent of the distribution of S , terms with $\Delta\tau \cdot \Delta S$ as coefficients must also disappear:

$$(2.26) \quad \langle r^2 \rangle \approx \left(\frac{\langle S \rangle}{\langle \tau \rangle} \right)^2 + \frac{\langle \Delta S^2 \rangle}{\langle \tau \rangle^2} + \langle \Delta\tau \rangle \frac{\langle S \rangle^2}{\langle \tau \rangle^4}$$

If we assume that ΔS is small, and define $\sigma_r^2 = \sigma_T \frac{\langle S \rangle}{\langle \tau \rangle^2}$, we get the standard deviation of the estimated rate:

$$(2.27) \quad \sigma_r = \sigma_T \frac{\langle S \rangle}{\langle \tau \rangle^2}$$

By invoking the scalar timing law (Weber-Fechner's law for temporal estimation) (Buhusi and Meck, 2005; Church, 2003; Gibbon et al., 1984), which has the form $\sigma_T = \alpha \langle \tau \rangle$, we obtain:

$$(2.28) \quad \sigma_r = \alpha \frac{\langle S \rangle}{\langle \tau \rangle}$$

Let us assume a simple case of constant firing rate over the period τ , and that the spike count depends on the parameter through a tuning curve $f(\theta)$ such that $\langle S(\theta, \tau) \rangle = f(\theta) \cdot \tau$. Using this, we get:

$$(2.29) \quad \sigma_r = \alpha \cdot f(\theta)$$

This implies that the noise of the rate variable is independent of the temporal window τ . We will now use a modification of Equation 2.17 (which was used in estimating the error of the decoded variable θ) where we use the deduced rate rather than the spike count:

$$(2.30) \quad \frac{\sigma_{\theta}(\theta, \tau_1)}{\sigma_{\theta}(\theta, \tau_2)} = \frac{\sigma_r(\theta, \tau_1)/f'(\theta)}{\sigma_r(\theta, \tau_2)/f'(\theta)} = 1$$

By taking the log of this expression, we clearly find that the *LJR* should have a slope of 0.

Now generalize this to a case where $\langle S(\theta, \tau) \rangle = f(\theta) \cdot g(\tau)$, where $g(\tau)$ is not the density, but rather the cumulative number of spikes between 0 and time τ . Like the constant firing rate case, we can retrieve $f(\theta)$ by dividing the spike count with $g(\tau)$. Note that in the constant firing rate case $g(\tau) = \tau$, so this formulation is equivalent to the constant firing rate case. Let's define this new variable $q = S(\theta, \tau)/g(\tau)$, which is an attempt to retrieve $f(\theta)$. Here, we will only examine the simple case where ΔS is very small and can be ignored.

$$q(\theta, \tau) = \frac{\langle S(\theta, \tau) \rangle}{g(\tau + \Delta\tau)} \approx \frac{\langle S(\theta, \tau) \rangle}{g(\tau) + \Delta\tau \cdot g'(\tau)}$$

(2.31)

$$\approx \frac{S(\theta, \tau)}{g(\tau)} \left(1 - \Delta\tau \left(\frac{g'(\tau)}{g(\tau)} \right)^2 \right)$$

Approximating the second moment:

$$\langle q^2(\theta, \tau) \rangle = \left(\frac{S(\theta, \tau)}{g(\tau)} \right)^2 \left\langle \left(1 - \Delta\tau \frac{g'(\tau)}{g(\tau)} \right)^2 \right\rangle$$

(2.32)

$$= \left(\frac{S(\theta, \tau)}{g(\tau)} \right)^2 \left(1 + \langle \Delta\tau^2 \rangle \left(\frac{g'(\tau)}{g(\tau)} \right)^2 \right)$$

The last stage is obtained because $\langle \Delta T \rangle = 0$. Therefore, the variance is:

$$(2.33) \quad \sigma_q^2 = \langle \Delta \tau^2 \rangle = \left(\frac{S(\theta, \tau)}{g(\tau)} \right)^2 \left(\frac{g'(\tau)}{g(\tau)} \right)^2$$

Per the scalar timing law $\langle \Delta \tau^2 \rangle = \alpha^2 \cdot \tau^2$, and using

$S(\theta, \tau) = f(\theta) \cdot g(\tau)$ we get that:

$$(2.34) \quad \sigma_\theta(\tau) = \frac{\sigma_q}{f'(\theta)} = \frac{\alpha \cdot f(\theta)}{f'(\theta)} * \frac{\tau \cdot g'(\tau)}{g(\tau)}$$

Consequently:

$$(2.35) \quad \frac{\sigma_\theta(\tau_1)}{\sigma_\theta(\tau_2)} = \frac{\tau_1 g'(\tau_1) g(\tau_2)}{\tau_2 g'(\tau_2) g(\tau_1)}$$

For a power-law $g(\tau) = \tau^\eta$ we get that this ratio is one, just like the constant firing rate case ($\eta = 1$).

The analysis above has been verified with a Monte Carlo simulation constructed within MATLAB. The simulation also demonstrated that, even though my assumption $\Delta \tau \ll \tau$ is biologically realistic (Buhusi and Meck, 2005), the conclusions of the above work hold for a wide range of $\Delta \tau$ values, up to and including $\Delta \tau = \tau$. This is demonstrated below in Figure 2.2.

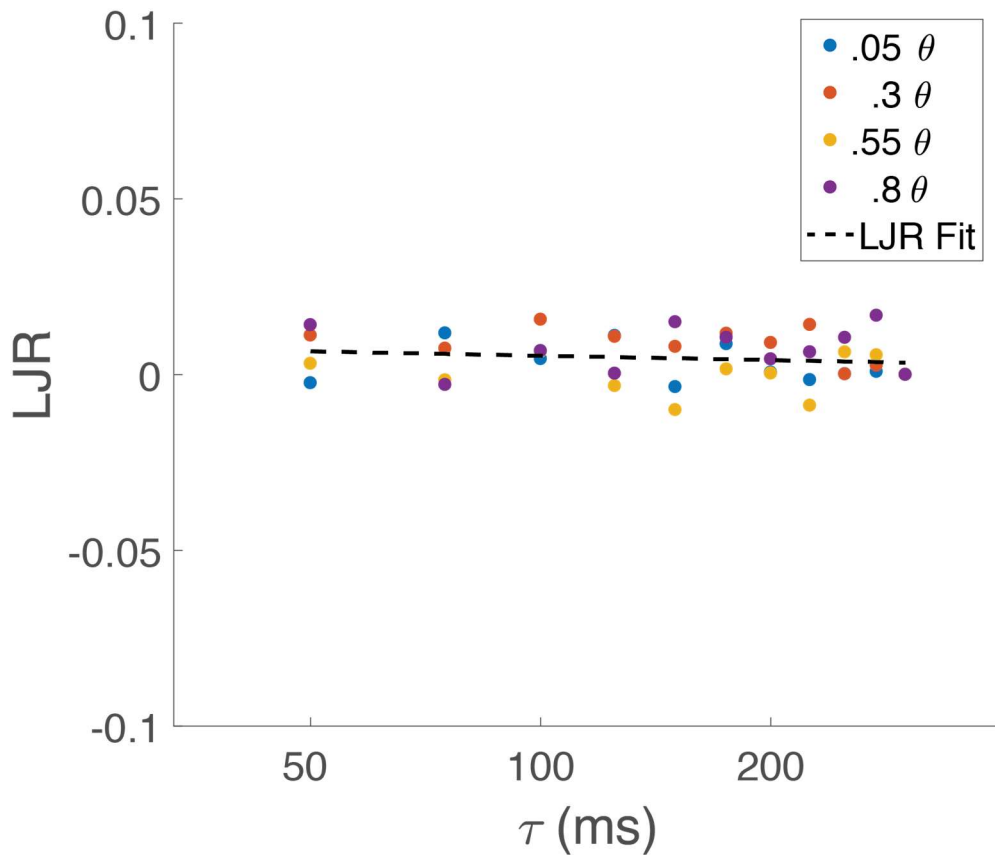


Figure 2.2: Demonstration of the effect of timing estimation errors

Above, I demonstrate a Monte Carlo simulation that shows what would happen if errors in time estimation were the primary cause of errors in sensory estimation. This simulation is run for multiple reference stimulus intensities (arbitrary units) to demonstrate that the effect holds for multiple sensory magnitudes. The derived LJR line has a slope of approximately 0; this denotes that, if timing issues were the cause of perceptual errors, we would see essentially no differences in error rate as we decreased the stimulus duration.

2.2.5 – Fitting stimulus magnitude and duration

While I have focused primarily on the effect that stimulus duration has on discrimination ability, the current theory also can be used to predict the scaling of the JND as we change the reference stimuli. Below, I analytically solve the functional relationship between JND, stimulus duration, and stimulus intensity.

2.2.5.1 – Analytical work

Previously, I have assumed that the behavioral data follows the Weber-Fechner law (see Chapter 1 or for an overview). While this is often the case, there are exceptions (Legge, 1981; McGill and Goldberg, 1968; Stevens, 1961). For this part of the analysis, I will derive a more generalized version of the equation for behavioral variability. To do this, I first must describe the noise scaling as the following (Shouval et al., 2013):

$$(2.36) \quad \sigma_{\theta}(\theta, \tau) = \alpha(\tau) \cdot \theta^{1-\phi}$$

where ϕ is acting a correction term for sensory modalities that do not align perfectly with the linear scaling of the Weber-Fechner law. If we look at the case of $\alpha(\tau) \geq \tau_{sat}$, we can build a tuning curve that will result in the behavioral variability that we desire (Shouval et al., 2013):

$$(2.37) \quad r_{sat}(\theta) = K \cdot \left(\frac{\theta^{\phi}}{\phi} - \frac{C^{\phi}}{\phi} \right)^n$$

where $K = \pm \beta / \tau_{sat} \cdot \left(\frac{1-\rho}{\alpha_{sat}} \right)^n$, $n = \frac{1}{1-\rho}$, α_{sat} is the Weber fraction at or above τ_{sat} , $r_{sat}(\theta)$ is the mean firing rate given a stimulus θ presented for τ_{sat} , ρ is the previously designated noise descriptor, τ_{sat} is the previously described saturation time, and β and C are constants that have no relevance to the analysis below.

However, the above is a constrained case, only relevant for stimuli whose durations are at or above τ_{sat} . To generalize to $\tau < \tau_{sat}$, we assume that for any window duration we

use the firing rate as described in Equation 2.37. A shorter duration, however, will affect the spike count, and scale it down by a factor of τ/τ_{sat} . To generalize, we need to adjust the tuning curve to fit stimulus durations below τ_{sat} . This is equivalent to scaling of the tuning curve function such that:

$$(2.38) \quad r(\theta) = \frac{\tau}{\tau_{sat}} \cdot r_{sat}(\theta)$$

where $r(\theta)$ is the generalized tuning curve for times below τ_{sat} . Using Equation 2.37, we can expand Equation 2.38 to:

$$(2.39) \quad \frac{\beta}{\tau_{sat}} \cdot \left(\frac{1-\rho}{\alpha(\tau)}\right)^n \cdot \left(\frac{\theta^\phi}{\phi} - \frac{C^\phi}{\phi}\right)^n = \frac{\tau}{\tau_{sat}} \cdot \frac{\beta}{\tau_{sat}} \cdot \left(\frac{1-\rho}{\alpha_{sat}}\right)^n \cdot \left(\frac{\theta^\phi}{\phi} - \frac{C^\phi}{\phi}\right)^n$$

Canceling out like terms, we are left with:

$$(2.40) \quad \frac{\beta}{\tau_{sat}} \cdot \left(\frac{1-\rho}{\alpha(\tau)}\right)^n = \frac{\tau}{\tau_{sat}} \cdot \frac{\beta}{\tau_{sat}} \cdot \left(\frac{1-\rho}{\alpha_{sat}}\right)^n$$

Simplifying further:

$$(2.41) \quad \alpha(\tau) = \alpha_{sat} \cdot \left(\frac{\tau_{sat}}{\tau}\right)^{1-\rho}$$

Combining Equation 2.37 and 2.41

$$(2.42) \quad \sigma_\theta(\theta, \tau) = \alpha_{sat} \cdot \left(\frac{\tau_{sat}}{\tau}\right)^{1-\rho} \cdot \theta^{1-\phi}$$

Rephrasing:

$$(2.43) \quad JND(\theta, \tau) = (\alpha_{sat} \cdot \tau_{sat}^{1-\rho}) \cdot \tau^{-(1-\rho)} \cdot \theta^{-(\phi-1)}$$

Note that when $\phi \cong 0$ and $\tau \geq \tau_{sat}$, the τ terms cancel out and Equation 2.43 becomes Weber-Fechner's law.

This equation makes a strong prediction. When we alter stimulus magnitude and duration, we expect a subject's JND to take on a double power law fit of the form:

$$(2.44) \quad JND(\tau, \theta) = \alpha_{fit} \cdot (\tau^{-x} \theta^{-y})$$

where the $\alpha_{fit} = (\alpha_{sat} \cdot \tau_{sat}^{1-\rho})$, $x = 1 - \rho$ and $y = \phi - 1$. This means that, once we find α_{sat} , τ_{sat} , ρ , and ϕ , we can make solid estimates on how JND increases as stimulus magnitude and duration decreases, and then compare it against the actual data.

2.2.5.2 - Monte Carlo verification

To verify the above analytical work, I built a basic Monte Carlo simulation. The simulation used twenty sigmoidal shaped pseudo-neurons that, through summation, approximated the tuning curve described in Equation 2.37. Each pseudo-neuron had its own sigmoid tuning curve with three parameters: a max firing rate, a slope, and a threshold. To start, each pseudo-neuron had randomized parameters; I used gradient descent methodology to alter their parameters such that the summation of the pseudo-neurons resulted in the appropriate tuning curve, which was dependent on the starting assumptions (i.e., α_0 , τ_{sat} , ρ , and ϕ). An example of this process is shown in Figure 2.3.

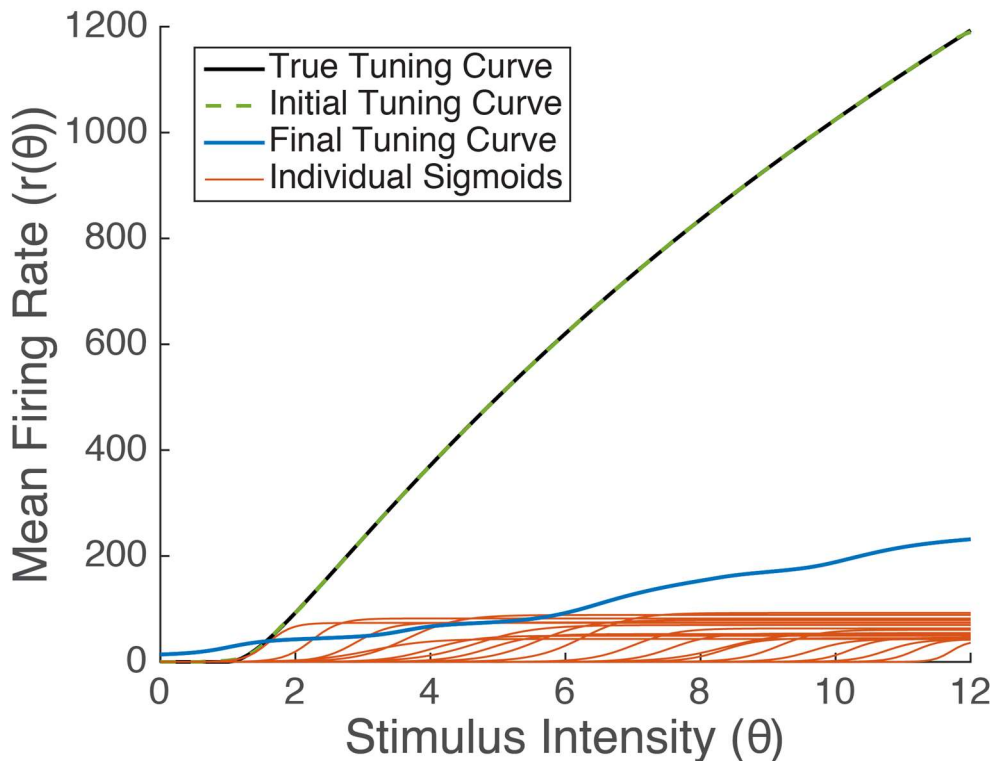


Figure 2.3: Applying gradient descent to build a tuning curve

Above, I have a demonstration of the gradient descent procedure used to build the tuning curve in the Monte Carlo simulation. The solid black line represents Equation 2.37, and is the function that the pseudo-neurons are attempting to replicate. The blue curve represents the summation of the initial states of the pseudo-neurons, whose parameters were chosen randomly. Over 2000 iterations of a gradient descent algorithm, the parameters of the pseudo-neurons were altered so that the sum of their functions would result in an estimation of Equation 2.37. The sigmoids with their final parameters are displayed in red. The dashed green line represents the final summation of the pseudo-neuron functions, resulting in an accurate estimation of the appropriate tuning curve. The above function represents the Poisson/Non-Weber condition (see Table 2.1 for condition descriptions).

Once suitable pseudo-neurons have been created, I simulated them in a traditional psychophysical experiment (see Chapter 1 or (Klein, 2001) for a brief overview). A series of reference and test stimuli were created, and ‘presented’ to the group pseudo-neurons. This process entailed that numerical values for these stimuli were inputted into the

sigmoid functions described above; the output of these functions correspond to that pseudo-neurons spike rate. This was multiplied by a stimulus presentation time (varied as a condition). The result was an average spike count, which was then used as the seed parameter for a randomized Poisson function; the output acted as the stochastic spike count of the cell. In summary, like a real neuron, a stimulus was presented and a semi-random number of spikes occurred in response.

For each simulated trial, the spike count of all 20 pseudo-neurons was summed, and the final count for the reference and test stimuli were compared. If the spike count for the test stimulus was higher than the reference stimulus, then the simulation was judged to have perceived the test stimulus as higher; otherwise, it perceived the test stimulus as lower. This process was repeated for thousands of times, and the results used to build a psychometric curve and determine the *JND* (See Figure 1.1) Plotting this on a 3-dimensional graph, I can fit the simulated data points to Equation 2.44. An example of this plot can be found in Figure 2.4.

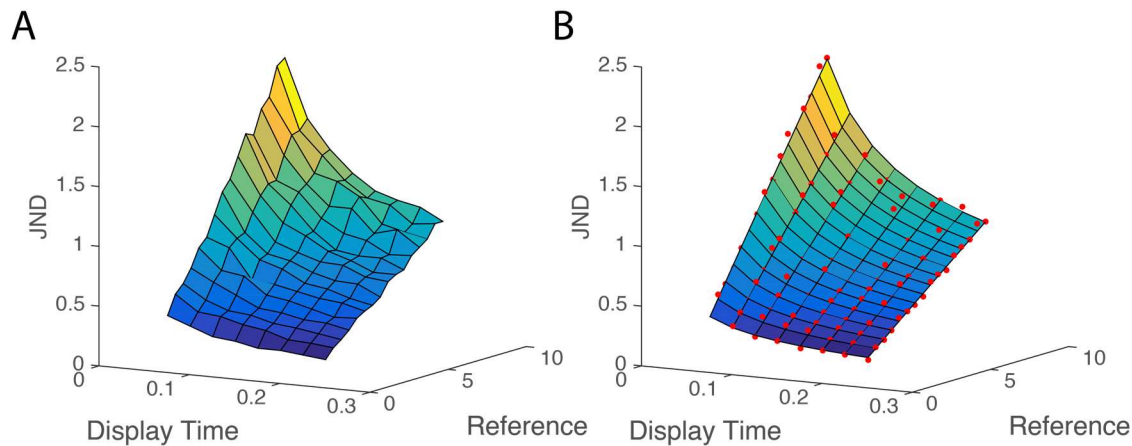


Figure 2.4: Simulation of psychophysical task using the derived tuning curve

The results above are from the Weber/Poisson condition. **A:** Above, we see a 3-dimensional representation of the output of the Monte Carlo simulation. The vertices of the projected surface represent the calculated JNDs for each stimulus duration and magnitude condition of the simulated psychophysical task. **B:** An alternative projection of the data. The red points represent the calculated JNDs, while the projected plane represent the best fit of the data, as calculated by the *nlinfit* function within MATLAB.

This fit was performed for the Monte Carlo results models of conditions: Poisson/Weber, Poisson/Non-Weber, Constant/Weber, and Constant/Non-Weber. All of these conditions had a $\tau_{sat} = 230 \text{ ms}$, and an $\alpha_{sat} = .075$. Descriptions of the variables ϕ and ρ in the different conditions are in Table 2.1 for ease of reference. Additionally, in the constant noise conditions, the simulation was altered to remove the Poisson noise of the neurons and add a constant Gaussian noise ($\mu = 0, \sigma = 1$) to each spike count. Simulated reference stimuli were ranged from 1.5 to 9 in .5 increments, for durations ranging from 50 to 250 milliseconds in 25 millisecond increments. Each condition was repeated for 1000 trials.

	α_0	τ_{sat}	ϕ	ρ
Weber/Poisson	.075	230 ms	0	.5
Weber/Constant	.075	230 ms	0	0
Non-Weber/Poisson	.075	230 ms	.5	.5
Non-Weber/Constant	.075	230 ms	.5	0

Table 2.1: Condition descriptions

A quick description of what the initial parameters of the different simulations that were run.

The parameters derived by fitting the simulation results to the double power law described in Equation 2.44 (results shown in Table 2.2) confirm the analytical solution, with some margin of error due to the stochastic nature of the simulation. For reference, the analytical solution suggests that $\alpha_{fit} = (\alpha_0 \cdot \tau_{sat}^{1-\rho})$, $x = 1 - \rho$ and $y = \phi - 1$.

	α_{fit}		x		y	
	Analytical	Simulated	Analytical	Simulated	Analytical	Simulated
Weber/Poisson	.036	.048 ± .0092	.5	.57 ± .048	-1	-.97 ± .079
Weber/Constant	.017	.030 ± .012	1	.98 ± .11	-1	-.93 ± .15
Non-Weber/ Poisson	.036	.050 ± .015	.5	.54 ± .088	-.5	-.48 ± .12
Non-Weber/ Constant	.017	.023 ± .0051	1	1.0 ± .065	-.5	-.55 ± .072

Table 2.2: Comparing Monte Carlo and analytical results

Records of the results from the Monte Carlo simulation, as compared to the predicted values from the analytical methods (Section 2.2.5.1). The distributions referenced above represent the 95% confidence interval.

2.3 – Conclusions

For an overview and an intuitive description of the model described in this chapter, read Section 2.2.1.

In this chapter, I built an analytical model from three simple assumptions, described in Section 2.2.1. This model makes several predictions, which will be discussed below.

2.3.1 – Neuronal noise as a source of perceptual error

Many people within the field of psychophysics believe that neuronal noise may be a source of perceptual error. This has an intuitive appeal – neurons have noisy firing rates, and it seems that this stochasticity may leave its mark on behavior. In this paper, I have taken this idea very seriously, and functionally described what this relationship should be in Equation 2.2, reproduced here for convenience

$$(2.2) \quad LJR = \log\left(\frac{JND_{\tau}}{JND_{sat}}\right) = (\rho - 1) \cdot \log(\tau) - (\rho - 1) \cdot \log(\tau_{sat}); \quad \tau < \tau_{sat}$$

where LJR is the Log-JND-Ratio (defined here), JN_{τ} is the JND for a time window of length τ , and JND_{sat} is the JND for $\tau \geq \tau_{sat}$. For $\tau > \tau_{sat}$, the $LJR = 0$.

Of particular importance in this analysis is the idea that different statistical distributions (Poisson, Gamma, Gaussian, etc.) will be effected differently by a reduction of a stimulus's duration. In general, neurons are characterized by a Poisson firing rate (Dean, 1981a; Kandel et al., 2012) (although there are exceptions (Zhong et al., 2005)). If this is the cause of behavioral variability (and if the assumptions stated in Section 2.2.1 hold), then Equation 2.2 necessitates certain behavioral relationships. The most important

relationship is that, if we were to perform a psychophysical experiment and plot the data for incrementally decreasing display times (Figure 1D), then we would expect the line created by Equation 2.2 to have a slope of -0.5 . Alternatively, if perceptual errors are not caused by neuronal noise, but rather some constant noise decoding process, we would expect a slope of approximate -1 .

2.3.2 – Errors in timing as a source of perceptual error

Errors in perception extend to time perception. There is a robust literature on the properties of errors in timing perception under the term *scalar timing* (Buhusi and Meck, 2005; Church, 2003; Gibbon et al., 1984). I addressed the possibility that scalar timing was the main contributor to perceptual errors. To quickly recap, if the decoding process for a spike train uses some measure of spike rate, then the length of the stimulus presentation would have to be known for that calculation. It is possible that, when the stimulus's duration is estimated, errors are introduced in the perceptual judgment. Using some basic assumptions (primarily that the timing errors are proportional to the length of time being measured), I found the following (see Section 2.2.4 for derivation): if temporal estimation errors were the primary cause of perceptual errors, then the predicted slope of the *LJR* graph (Figure 2.1D) should approach 0. This was also confirmed by Monte Carlo simulations, even for large errors in the temporal window estimation.

2.3.3 – Predicting JND as a function of stimulus magnitude and duration

The analytical work in 2.2.5.1 extends my predictions beyond the temporal domain. While Equation 2.2 deals with what happens as we change the presentation time, I extend this

to show what will happen as we adjust both stimulus magnitude and duration. In order to do this, I had to introduce another variable (ϕ) that generalized the model to work with stimulus modalities that did not perfectly fit Weber-Fechner's law. Following this, I derived a double power law function (Equation 2.44) that makes predictions on the JND as a function of stimulus magnitude and duration (Table 2.2). These predictions, and the other mentioned above, will be compared against the experiment done in Chapter 3.

CHAPTER 3: CONTRAST DISCRIMINATION UNDER TEMPORAL CONSTRAINT

3.1 – Introduction

The results of the previous chapter show that it is possible to infer key statistical properties of the neural noise that generates perceptual errors simply by altering the viewing time of the stimulus. While it is possible to make a psychophysical experiment on any sensory modality, I have chosen contrast stimuli as the sensory modality to study. First, to satisfy the second assumption of my model, the tuning curve for contrast sensitive neurons is monotonic (i.e., as the contrast intensity increases, so does the firing rate of contrast sensitive neurons) (Dean, 1981b). Second, the spike count variability is well established in contrast sensitive neurons (Dean, 1981a), satisfying assumption three in my theory. Additionally, contrast psychophysics is a well-developed field and its protocols are well established (Snowden et al., 2012).

The core of the experiment presented here is how perceptual errors increase as we decrease the time the stimulus is displayed. The psychophysical literature has seen seemingly similar experiments (Bloch, 1885; Gorea, 2015; Gorea and Tyler, 1986; Legge, 1978; Schofield and Georgeson, 2000; Watson, 1979), but there are key distinctions between those experiments and mine. The famous psychophysicist Bloch conducted one of the first experiments that controlled stimulus duration (Bloch, 1885; Gorea, 2015). His results showed that, for durations shorter than 50ms, subjects conflate duration and brightness such that a short duration, high brightness stimulus is perceptually indistinguishable from a longer duration, lower brightness stimulus. The physiological explanation for Bloch's law arises from the properties of retinal neurons, and is valid only for limited durations. In contrast, here I use stimuli with durations longer than 50ms, which

subjects can estimate both magnitude and duration for separately. Additionally, Bloch used brightness rather than contrast as the sensory modality of his experiment.

Other previous experiments have examined the effect of contrast stimulus duration over intervals longer than 50 ms (Gorea and Tyler, 1986; Legge, 1978; Schofield and Georgeson, 2000; Watson, 1979). However, these experiments were not based on the theoretical foundation developed here, and used experimental techniques that would not adequately test aspects of the current model. The cited studies were primarily interested in the threshold detection of subjects (i.e., whether a weak contrast stimuli can be detected at all). In the current study, instead of studying detection thresholds, I studied discrimination thresholds; subjects were asked to discriminate which of two gratings had a higher contrast, rather than whether contrast was present or absent. This change allows us to study how trial-by-trial spike variance can affect discrimination ability as the reference stimulus was changed (see Section 2.2.5 for more details). Nevertheless, when interpreted with my theoretical framework, their results are largely consistent with my observations and are discussed in Section 3.4 of this chapter.

3.2 - Methods

All work was carried out in accordance with the Code of Ethics of the World Medical Association (Declaration of Helsinki), and informed consent was obtained from all volunteer subjects.

3.2.1 - Experimental Design

A group of nine visually normal subjects (Age range: 20-45, 5 female), two of which were disqualified for poor performance, were placed in a darkened room and instructed to place

their chin on a chinrest .91 meter from the screen. To deal with height differences among subjects, the headrest was vertically adjustable, and subjects were permitted to adjust it as needed during the experiment. Stationary gratings were presented with a randomized phase and a spatial frequency of 1 cycle/degree of vision. Each trial consisted of a sequence of six images: a randomized visual mask, a reference contrast grating, another mask, a test contrast grating, a final mask, and a prompt (See Figure 3.1A). During the prompt part of a trial, subjects were instructed to answer the question “Did the second grating have higher contrast than the first?”. Upon answering, subjects received feedback on whether their response was correct, followed immediately by the next trial. To prevent users from reliably using information from visual afterimages, checkerboard masks were presented for .5 seconds both prior to and following the stimuli, independent of the timing condition. The high contrast checkerboards had the additional benefit of keeping the subject in approximately the same contrast adaption state throughout every trial (Heinrich and Bach, 2001).

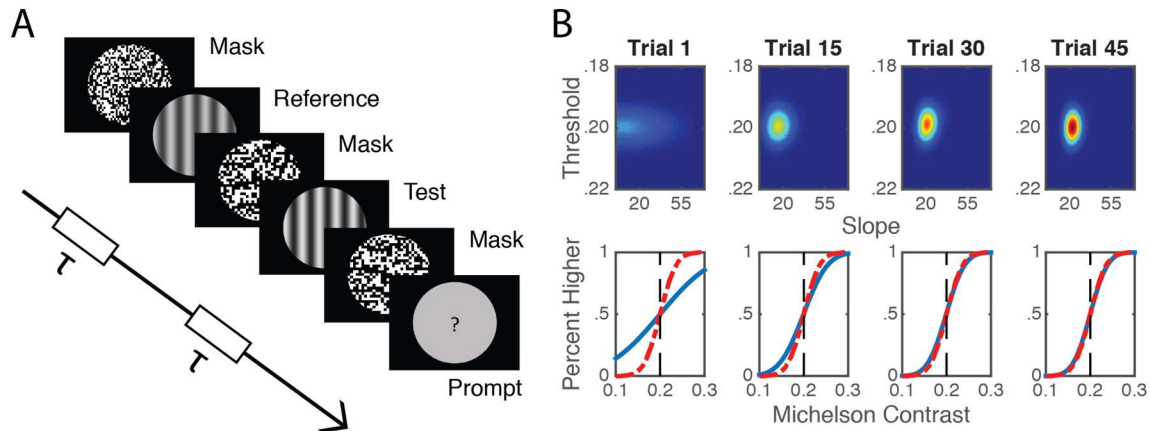


Figure 3.1: Experimental Methods

A: A reference grating and a test grating were presented for τ ms, each separated by a randomized checkerboard mask. The subjects were instructed to determine if the second stimuli had a higher contrast than the first. Display times of the gratings (τ) and contrast levels were manipulated as variables. **B:** (An animation is available at ‘www.goo.gl/hQIXO0’) To more effectively collect data, an adaptive algorithm was used that adjusted the slope and threshold (i.e. where the line crossed the 50 per cent mark) of the psychometric function on a trial-by-trial basis. For each trial within a condition, the algorithm updates the joint posterior distribution (image –top; video - left) of the estimated slope and threshold of the psychometric function (image – bottom; video - right). Here I have displayed a Monte Carlo simulation of the experiment (See Section 3.2.2.4 for more details), where the dashed red line is the ‘true’ simulated psychometric curve, and the blue solid line is the estimated curve. The posterior distribution parameters converge on the correct curve over the course of 45 simulated trials.

Each condition was defined by the presentation time and the reference contrast. Reference and contrast stimuli were presented for either 600, 300, 150, 125, 100, 75, or 50 ms. The reference contrast was presented as a random phase sinusoidal grating with a median brightness of 26.80 lumens, and a peak-to-peak magnitude of 3.50, 8.74, 13.98, 19.22, and 24.47 lumens. For each trial within a particular condition, the test stimulus contrast intensity was chosen using an adaptive algorithm.

3.2.1.1 - Hardware Setup

Subjects were seated in a darkened room in front of a Hitachi SuperScan 21 Supreme CRT Monitor (Hitachi, Tokyo, Japan). The monitor provided the only source of illumination in the room. A Pentium 4, 3 Ghz Windows XP SP2 computer controlled the screen with a Cambridge Research Systems VSG2/5 graphics card (Cambridge Research Systems, Rochester, UK), which refreshed the monitor at a rate of 80 Hz and a resolution of 769X1024. The screen's width was 34.8 cm. A black cardboard sheet was placed in front of the screen with a 12-inch diameter circle cut out of it to avoid subject's seeing the edge of the screen. This is due to distortion effect at the edge CRT monitors that may otherwise alter the stimuli. At least 5 minutes prior to every session, the screen was turned on to give it time to warm up and adjust the components to their operating temperature. The experiment was written and executed within MATLAB 2011B, and made heavy use of PsychToolbox-3, as well as functions provided by Cambridge Research Systems.

3.2.1.2 - Training

Subjects were trained prior to the task using a PowerPoint demonstration to familiarize themselves with what they were going to see. Following this initial training, they were given a shortened form of the normal task and asked to demonstrate that they understood what they were being asked to do. Subjects who performed below 70% accuracy on the training task were assumed not to have understood the directions, and given further instruction until they performed satisfactorily.

3.2.1.3 - Stimuli

Subjects were presented with two sinusoidally defined gratings on the monitor, and asked to determine which one had a higher contrast. The gratings were presented as having 1 cycle/degree of vision. This spatial frequency was chosen to correspond with Dean (1981a, 1981b), from which I have drawn my value for ρ to compare my results against (See Chapter 2 for discussion on ρ). Luminance of the gratings could range from 9.32 to 44.27 lumens, and the average intensity was 26.80 lumens, for all gratings. The full range of the monitor (0-46.6 lumens) was not used due to empirically determined distortion effects at these extended levels. The gratings were always presented vertically, and a random phase was chosen for each presentation.

To prevent subjects from having afterimages of the gratings (and therefore potentially integrating additional information after the grating was no longer presented), a randomized checkerboard pattern was used to mask the grating. The checkerboards were presented at the start of the trial, and presented for 500 ms each after the display of the reference and test gratings. Every presentation was independently randomized (i.e., each square could either be black or white, and was determined by a random number generator) to prevent subjects from being able to predict what they were going to see at each spot.

Throughout the whole experiment, including the checkerboard masks, the average luminance of the screen was designed to be 26.80 lumens. This was to maintain the same

level of light adaptation throughout. The monitor brightness levels were verified several times throughout the data collection phase using a Tektronix J17 LumaColor meter with a J1803 luminance head, and did not vary substantially from month to month.

The stimuli were varied over two conditions: reference magnitude and display time. The reference gratings, which fluctuated sinusoidally around the mean intensity of 26.80 lumens, had a peak-to-peak magnitude difference of 3.50, 8.74, 13.98, 19.22, and 24.47 lumens. Both the reference and test stimuli were presented at 600, 300, 150, 125, 100, 75, and 50 ms. The experiment was performed in blocks of 45 trials, each with a fixed reference contrast and duration, but varying test contrast. Each block was performed at least twice to counter-balance any order effects – one block had the reference stimuli prior to the test stimuli, and the other reversed this (see Section 3.3.3 for analysis of order effects). A Bayesian adaptive algorithm, described in detail below, was used during each block to determine the level of the test contrast stimuli.

We made an exception to the counterbalancing guideline in the 600 ms condition. It was added later in the testing protocol, and was only tested in the ‘reference first’ variation because previous testing had not suggested any choice bias. The order of these condition blocks was randomized to prevent behavioral variation between data collection days from affecting global analysis.

3.2.2 – Adaptive Algorithm

For this experiment, using traditional techniques to estimate the psychometric function would have required upwards of 30,000 trials for each subject. To reduce the number of trials needed, an adaptive algorithm was chosen to more efficiently gather data. Several adaptive methods exist within the literature (Leek, 2001), with benefits and drawbacks. Due to recent concerns about the convergence of traditional staircase procedures (García-Pérez, 1998), I chose to use a modified version of Kontsevich and Tyler (1999) for the current experiment (see Section 3.2.2.1 below for details on the modifications).

To summarize the method, an extremely wide prior probability was established for the psychometric function's slope in each condition, with a mean based on preliminary data. From this prior distribution, a test stimulus was chosen via an entropy based cost function to maximize the amount of information gained from the subject's response. Upon response, the priors were updated with the new information, and a new test stimulus was chosen. This was repeated for 45 trials per condition (see Figure 3.1B for a graphical representation).

3.2.2.1 - Bayesian adaption algorithm alterations and set up

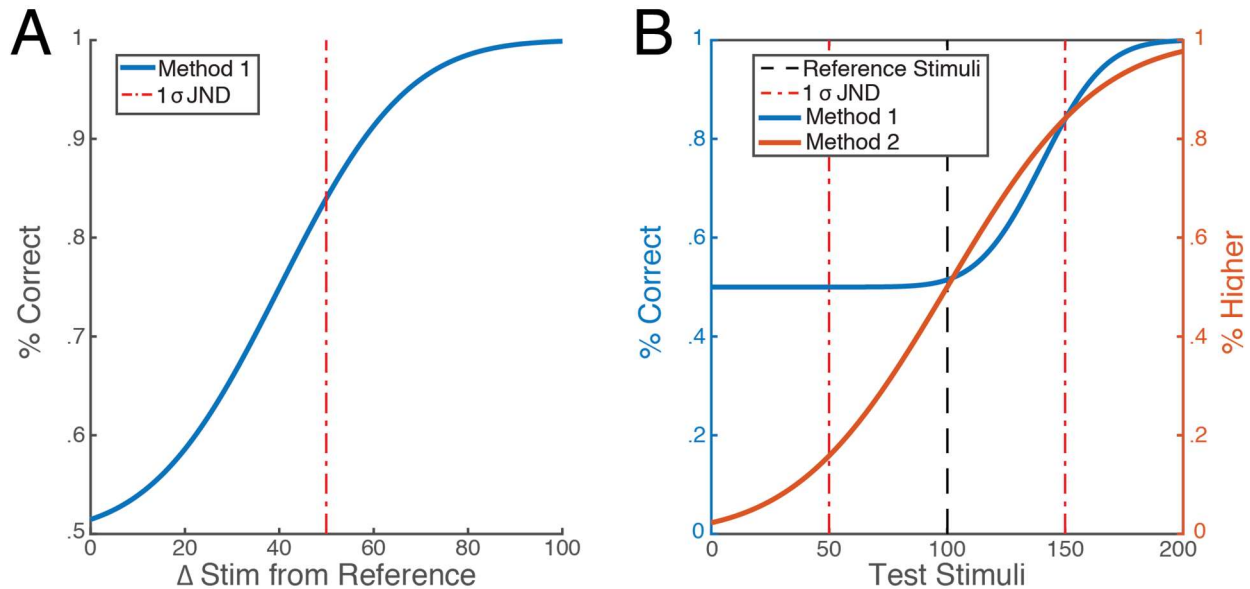


Figure 3.2: Alterations from Kontsevich and Tyler (1999)

The psychophysical literature has a diverse method for creating psychometric curves. Two prominent methods involving the use of sigmoids are displayed here. In both cases, a variety of test stimuli are presented in tandem with the reference stimuli, and the response of the subject is recorded. **A.** The subject's responses are coded as either right or wrong for the various test conditions, and test conditions are categorized by absolute difference from the reference stimuli. A sigmoid is then fitted to the data. This is the method that Kontsevich and Tyler developed (Kontsevich and Tyler, 1999) originally programmed for. **B.** The raw response of the subject ("Is the test stimuli higher or lower than the reference stimuli?") is plotted on the Y-axis instead of 'percent correct'. For mathematical simplicity, this is the line I fitted my data to. The solid blue line is the superimposition of Figure 3.2A. Note that the two lines, while similar above the reference stimuli magnitude, are not the same.

Several modifications had to be made to the methods described in Kontsevich and Tyler (1999) to connect it with the theory developed in Chapter 2. First, the range of the sigmoid JND function was adjusted from $[.5 \ 1]$ to $[0 \ 1]$; this can be interpreted as changing the Y-axis from 'percent correct' to 'percent perceived as higher'. See Figure 3.2 for a description and graphical representation of the differences between these two methods. Both methods are used somewhat interchangeably within the psychophysical literature, which can cause significant confusion.

The following equation represents the function that my algorithm optimizes for:

$$(3.1) \quad \psi(\theta) = \frac{1 + \operatorname{erf}(\beta \cdot (\theta - T))}{2}$$

where the psychometric function ψ represents ‘percent of time perceived as higher’, θ is the magnitude of the stimulus. The two variables β (the slope) and T (the threshold) are the variables that the adaptive algorithm changes to better fit the psychometric function of the test subject. At the start of every experimental condition, prior probability distributions were constructed for β and T . These distributions (seen in Figure 3.1B) can be interpreted as the initial guess (and the confidence in that guess) as to what β and T will be. These probability distributions are updated over the course of the experiment based on the accuracy of the subject at sensory discrimination. Preliminary data suggested little or no bias in user responses (i.e., the user was equally likely to be correct for test stimuli both above and below the reference stimuli), and behavioral data from the experiment confirmed this assumption (see Section 3.3.3). Thus, the prior for the threshold was chosen to be very narrow. Since my primary goal was to determine the slope of the curve, a very broad, nearly flat distribution was used for β . A copy of the code used, as well as the raw data from subjects, is available upon request.

3.2.2.2 – Convergence and exclusion criteria

A known issue with adaptive tests is that, if the prior assumptions are far from the correct solution, there can be a failure to converge within the number of trials allotted. To deal with this, test blocks where performance was below 80% or above 95% accuracy were excluded from analyses. Two subjects who performed below the 80% threshold in over

half their experimental blocks were excluded entirely from the analysis under the assumption that they were guessing randomly for large parts of the experiment.

3.2.2.2 - JND Value

Typically, within the psychophysical literature, JND is defined as the difference between the reference stimulus and the test stimulus that the subject perceives as higher 75% of the time. The 75% point is arbitrary, and has been eschewed in this paper to make the math easier. Discussion of JND throughout the rest of the paper is defined as 84%, which corresponds to the first standard deviation above and below the reference stimuli for a Gaussian distribution. Since the Bayesian adaptive algorithm determines the slope and threshold of the psychometric function, rather than a specific point, it would be computationally trivial to switch between the 75% and 84% JND if it were necessary for future comparisons.

3.2.2.4 – Proof of convergence through Monte Carlo simulation

Within their paper, Kontsevich and Tyler (1999) provided a great deal of support for their work, which will not be reproduced here. However, I have made modifications to their suggested algorithm; while these justifications are well founded, it is prudent test the algorithm to show that there are no unexpected consequences of my modified assumptions.

As described in Section 3.2.2.1, the main features that my algorithm adapts for are the slope (β) and threshold (T) of the psychometric function (Equation 3.1). For clarity, we will call the true values of these variables β_{true} and T_{true} . At the start of each experimental condition, the adaptive algorithm is given a prior probability distribution for β and T , which I will denote as β_{prior} and T_{prior} . These distributions can be interpreted as the adaptive algorithms initial ‘belief’ (and confidence about that belief) about what β_{true} and T_{true} are (see Figure 3.1B for a graphical representation). Over the course of the experiment, the algorithm updates the prior distributions based on the responses of the subject. Essentially, the algorithm starts with a (potentially wrong) belief, and converges onto the correct answer. Here, I develop a Monte Carlo simulation to test for this convergence in a variety of conditions.

To build this simulation, I took the code developed for the experiment and inserted a simulated subject. This simulated subject was essentially a psychometric function (see Equation 3.1) whose slope (β_{true}) and threshold (T_{true}) I controlled. Each trial, the simulation was presented with a numerical value (θ), which represented the contrast intensity that would have been shown to a real subject. θ was then inputted into the psychometric function ($\psi(\theta)$), and it returned the probability that the computer would respond ‘Yes’ to the prompt ‘Was the second stimulus greater than the first?’. A random number was generated, and if it was less than the returned value, the simulation recorded a ‘Yes’; otherwise it recorded ‘No’.

This simulation can be run with a variety of different conditions for the simulated subject's psychometric curve (β_{true} and T_{true}), as well as different prior probabilities for the adaptive algorithm (β_{prior} and T_{prior}). In Figure 3.3, I demonstrate several simulations on the convergence rate of β . Three different simulated subjects are presented, with a wide (yet plausible) range of β_{true} . Additionally, I present two different sets of β_{prior} - one where β_{prior} is 40% less than β_{true} , and one where it is 40% more. In all cases, I show that it converges on to the true answer within 45 trials, and often before. This result extends to all realistic conditions.

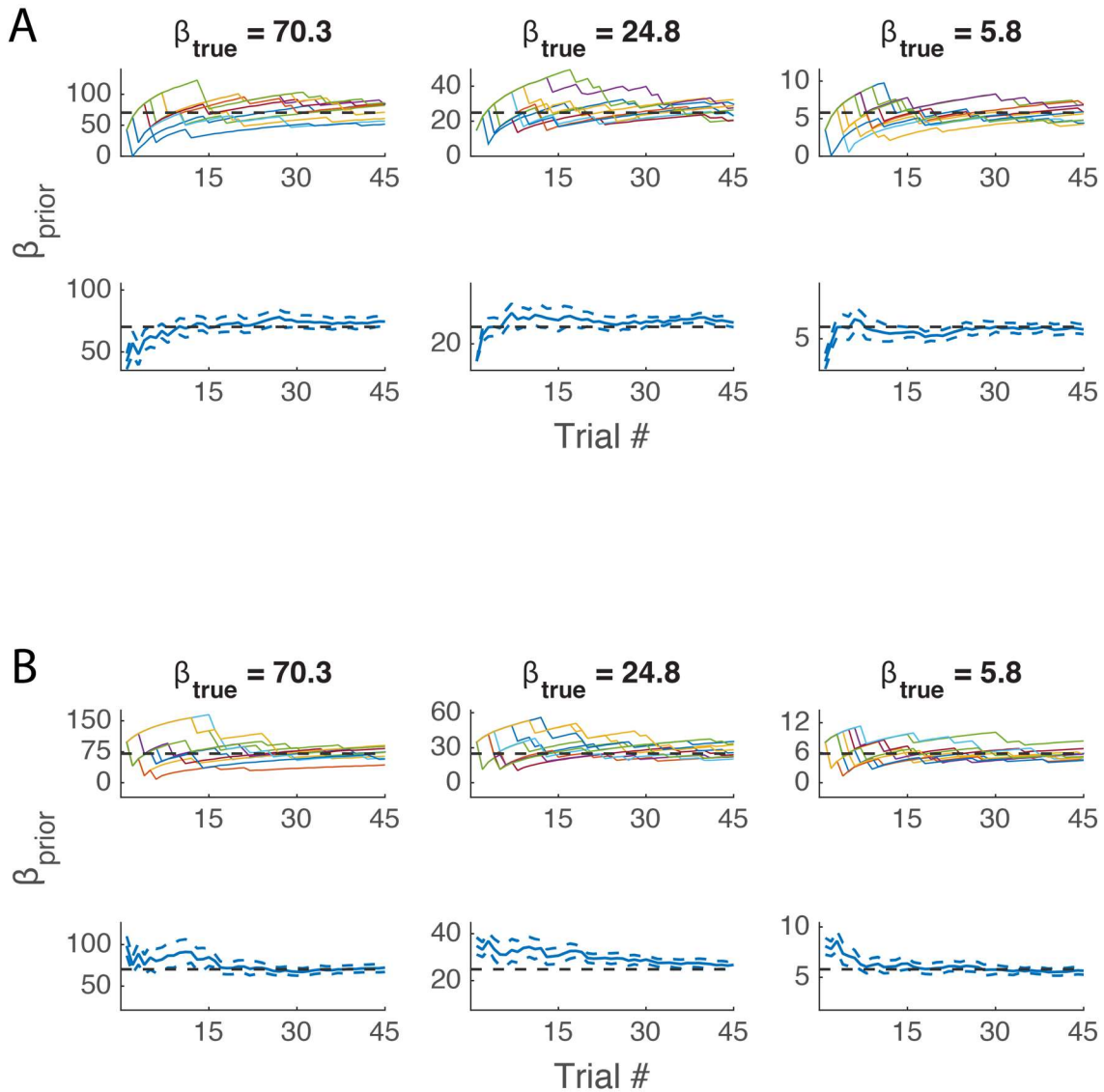


Figure 3.3: A Monte Carlo simulation of the adaptive algorithm

A: Here, we see a Monte-Carlo simulations of the adaptive algorithm over 45 trials, which are marked on the X-Axis. On the top graphs, I have 10 simulations overlaid on top of one another (separate lines), with the value for β calculated as being most probable shown on the Y-Axis. The dashed black line is the true value of beta, i.e., the value for the simulated responder described in Section 3.2.2.4. Note that the three graphs at the top have separate values for the true value of β , denoted in their titles. For all three graphs, the prior estimate of β started 40% below the true value of β . The three graphs on the bottom show a mean of calculated β (solid line) for the 10 simulations above, and the standard error (dashed lines) for the same. These graphs give a better insight on the average course of the convergence. **B:** This set of graphs show the same thing as **A**, with the only difference being that the starting prior estimate of β set at 40% above the true value of β .

Similar results were found for threshold, albeit with slower convergence rates. However, this is not an issue for the current experiment. While the threshold of the psychometric function is also technically being converged on, I did not expect it to change substantially. In behavioral terms, the only time that the threshold (T) would shift would be if there were a bias in the ‘Yes/No’ response. No such bias was found in any of the preliminary data collected. With this in mind, the prior probability distribution for T was set very narrowly; this has the side benefit of reducing the probability space calculated over, therefore increasing the rate of convergence for β . An analysis described in Section 3.3.3 (which discusses bias in the experimental data) demonstrated that this was a correct assumption.

3.2.3 - Calculating JND Related Measures

To quickly recapitulate the main point of Chapter 2, I developed a model that made a specific prediction relating the characteristics of neural noise to perceptual errors. This prediction is made explicit in Equation 2.2, copied below for reference:

$$(2.2) \quad LJR = \log\left(\frac{JND_{\tau}}{JND_{sat}}\right) = (\rho - 1) \cdot \log(\tau) - (\rho - 1) \cdot \log(\tau_{sat}); \quad \tau < \tau_{sat}$$

where LJR is the Log-JND-Ratio (defined here), ρ is the neuronal noise characteristic, JND_{τ} is the JND for a time window of length τ , and JND_{sat} is the JND for $\tau \geq \tau_{sat}$. For $\tau > \tau_{sat}$, the $LJR = 0$. The current experiment allows us to determine JND_{sat} and, using that, the LJR , τ_{sat} and ρ .

For each condition combination, the Bayesian algorithm converged on the correct slope and threshold of the psychometric function. To determine JN_{τ} , I found the stimulus value that would correspond to 84% ($\sim 1\sigma$) on the determined psychometric function. JND_{sat} (necessary for solving Equation 2.2) was found by averaging the JN_{τ} for the 300 and 600 ms conditions. These time values are presumed to be above τ_{sat} because JN_{300} and JND_{600} are statistically indistinguishable from one another when combined across all subjects (*unpaired t-test*, $p = 0.28$). JND_{sat} was calculated individually for each subject.

Once established, the value of JN_{sat} permits us to calculate the LJR (see Equation 2.2) for each subject and condition (Figure 3.4). For each subject, I used a non-linear fitting procedure (the *nlinfit* function within MATLAB) to fit the data to Equation 2.2 and extract the parameters τ_{sat} and ρ . Several distinct fitting methods were used and yielded similar results.

3.3 - Results

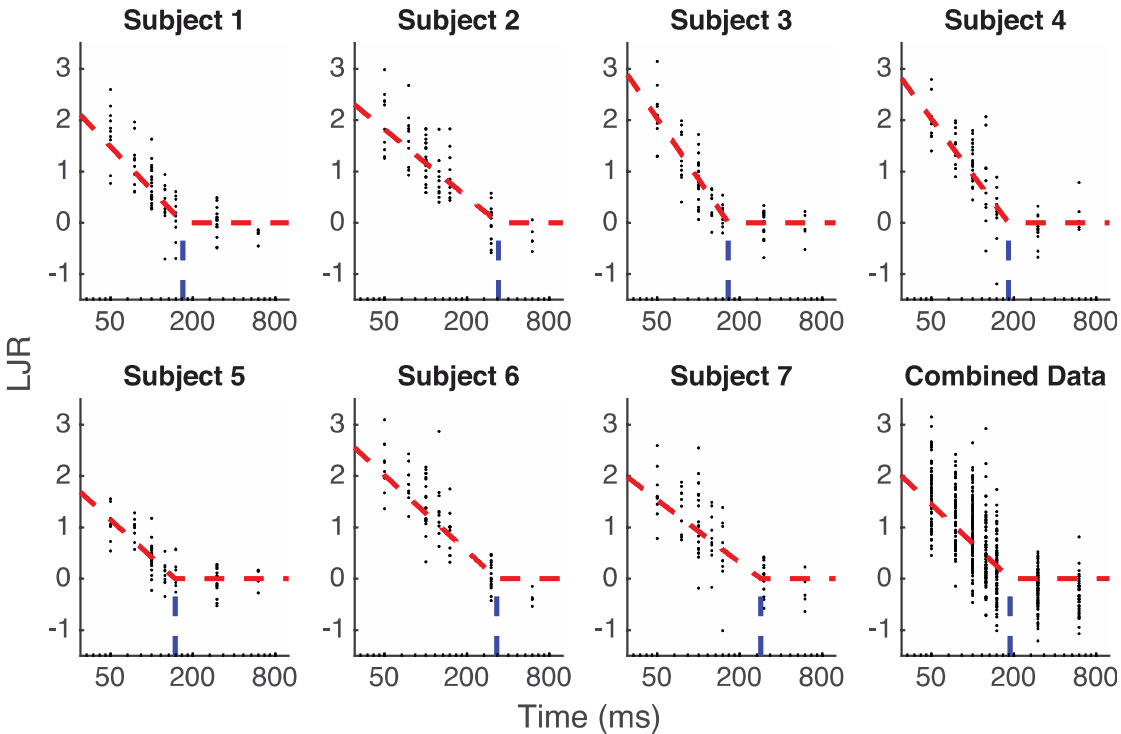


Figure 3.4: Individual and combined Log-JND-Ratio plots

Above, we have plotted the individual subject data along with the best fit line for Equation. 2. The calculated τ_{sat} is denoted by the dashed blue line, and ρ (the noise term) is equivalent to the slope of the initial segment of the line plus one. The final graph, 'Combined Data', brings together all of the data from every subject, and also finds the best fit for Equation 2.

3.3.1 - Primary results

The theoretical analysis in Chapter 2 relates the statistics of perceptual errors to the statistics of the neural code. Specifically, I noted how perceptual errors would vary with changes to the window of temporal integration given different models of noise. On the basis of this theory, I designed an experiment to test if the source of perceptual errors is indeed the variability of the encoding sensory neurons, as is suspected in much of the

literature (Britten et al., 1993, 1996; Cohen and Newsome, 2009; Mazurek et al., 2003; Shadlen et al., 1996; Shouval et al., 2013).

The perceptual errors of my subjects were tested in a contrast discrimination task for different durations of stimulus presentation and different contrasts. The results of each subject (shown in Table 3.1 and Figure 3.4) were fit separately to Equation 2.2 (dashed red line in Figure 3.4). Taking the inter-subject statistics (i.e., averaging across the values calculated for each subject), I found the average of the slope on the log-log plot to be approximately -1.2, which implies that $\rho = -0.20 \pm 0.31$. This value of ρ is significantly different ($p \cong .00014$) from the Poisson-like value of $\rho = .58$ found through an electrophysiology experiment (Dean, 1981a). However, it is statistically indistinguishable from a constant noise condition ($\rho \cong 0$). I also found that $\tau_{sat} = 232 \pm 83$ ms (Figure 3.4 and Table 3.1). Note that this value of τ_{sat} is consistent with the estimation of JND_{sat} done in Section 3.2.3, which showed τ_{sat} should be less than 300 ms. Similar results are also derived and presented in both Table 3.1 and Figure 3.4 under ‘Combined Data’ by combining all the data points across subject, time, and reference conditions, and fitting Equation 2.2.

Individual Data	$\tau_{sat} (ms)$	$SE_{\tau} (ms)$	ρ	SE_{ρ}
Subject 1	169.22	13.17	-0.2180	0.1551
Subject 2	339.73	38.55	0.0496	0.0984
Subject 3	165.09	9.50	-0.6990	0.1492
Subject 4	182.85	14.98	-0.5598	0.1815
Subject 5	148.42	12.27	-0.0571	0.1486
Subject 6	330.60	29.57	-0.0661	0.0949
Subject 7	284.93	71.17	0.1184	0.1976
Combined Data	211.20	12.19	-0.1057	0.0774
Inter-subject Statistics	$\mu_{\tau} (ms)$	$\sigma_{\tau} (ms)$	μ_{ρ}	σ_{ρ}
	231.55	83.62	-0.2046	0.3111

Table 3.1: Summarized data from each subject

Here, we see the calculated τ_{sat} and ρ , along with their standard error, for each subject. To do analysis of the data, I have taken two approaches. First, under 'Combined Data', I have combined the derived LJR for every subject, time, and reference condition; following that, I fit Equation 2 to this cluster of data and extracted τ_{sat} and ρ . Second, under Inter-Subject Statistics', I simply averaged the values of τ_{sat} and ρ found for each subject.

Further, I have done analysis across the different reference contrast levels to tell if there is any trend relating the reference contrast stimulus to the resulting ρ or τ_{sat} values. Largely, I find that no such effect exists, except for the lowest contrast level (see Figure 3.5). At extremely low contrast intensities, subjects see a significant reduction in both ρ and τ_{sat} . This could be taken as evidence that different processes rule at extremely low contrast intensities, but further research should be done at the edges of perception.

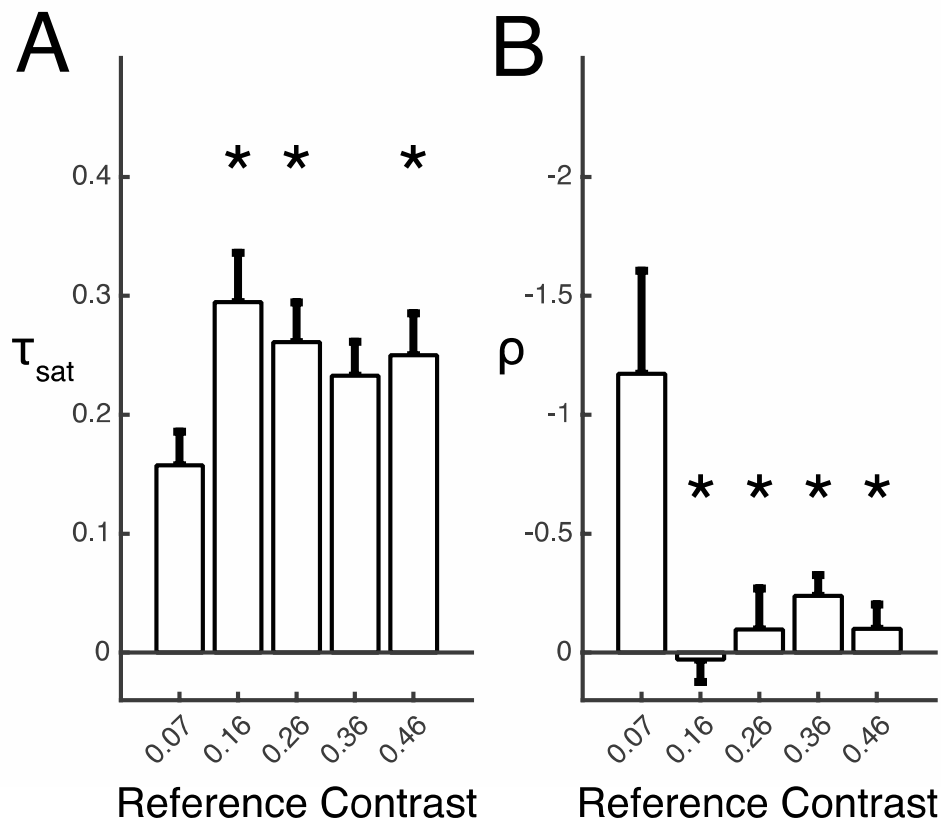


Figure 3.5: ρ and τ_{sat} values across reference contrast conditions.

In both charts, contrast is measured via Michelson Contrast. **A:** The dependence of τ_{sat} on the reference contrast magnitudes. **B:** The dependence of ρ on the reference contrast magnitudes. Values were obtained by taking the mean across all subjects within a reference condition. Significant differences ($p < .05$) were only found by comparing to the lowest reference contrast level, and are denoted by a *.

3.3.2 – Testing with respect to scalar timing

My analysis above assumed that spike counts are the primary feature being decoded, and that the spike counts for the reference and test stimuli are being compared during decoding. However, since we can distinguish between a short but intense grating and a long but weak grating (beyond 50ms) (Bloch, 1885; Gorea, 2015), the time of the stimulus presentation must also be known or inferred. If the decoding mechanism is provided with

an estimate of stimulus duration, it can calculate the spike rate and then infer the contrast intensity. It is, however, well established that timing perception is also prone to errors and that these errors increase linearly with the magnitude of the stimulus in an effect called scalar timing (Buhusi and Meck, 2005; Church, 2003; Gibbon et al., 1984). In Section 2.2.4, I found that for any system that had the stimulus estimation errors derived primarily from errors in temporal estimation, the predicted slope of the LJR graph (i.e., Figure 3.4) would approach 0. This result is obviously inconsistent with my data (with a slope of approximately -1.2), and suggests that timing related errors make an insubstantial contribution to perceptual errors (σ_θ).

3.3.3 – Bias and order preference

In psychophysical experiments, it is important to make sure that the experimental paradigm does not lend itself to systematic errors. In the case of the current experiment, there are two controls that I performed to guard against these. In the first control, I wanted to make sure that subjects were not more inclined to select ‘yes’ rather than ‘no’ when prompted with “Was the second stimulus higher than the first?”. To find this out, I looked at the response characteristics of each subject. In Table 3.2 below, I have recorded the percent of time that subjects responded ‘yes’ in both the normal condition, where the reference contrast is presented before the test condition, and the reverse condition, where the opposite is true. Testing with a *one-sample t-test*, I failed to reject the null hypothesis (i.e., that the data is not biased in a statistically significant way) in the normal condition ($p = .93$), the reverse condition ($p = .19$) or a combination of the two conditions ($p = .37$). This failure to reject suggests that there is no bias in response.

	Subj. 1	Subj. 2	Subj. 3	Subj. 4	Subj. 5	Subj. 6	Subj. 7	Combined
Normal Condition	0.50	0.49	0.49	0.48	0.54	0.50	0.49	0.50
Reverse Condition	0.52	0.49	0.49	0.53	0.53	0.56	0.49	0.52
							Total	0.51

Table 3.2: Measurements of bias

The table above records the probability that a subject will respond ‘Yes’ to the prompt ‘Does the second grating have a higher contrast than the first?’. Every subject responds in an unbiased manner.

In my second control for systematic errors, I looked at the possibility that subjects might have an order preference for stimuli – i.e., the first grating presented may consistently be perceived as higher or lower than the second. To test against this, halfway through the test the reference and test gratings were switched without informing the subject. Calling back to Table 3.2, I used a *two-sided t-test* to test between the normal and reverse conditions, and failed to reject the null hypothesis (i.e., that the two conditions are statistically indistinguishable) at a $p = .26$. This bolsters the hypothesis that there was no effect of order.

In addition, we have looked at the calculated JND across all subjects. If there were an order effect, we would have expected to see differences between the normal and reverse presentations. In Table 3.3, I have recorded the average and standard deviation of the JND in every time and reference condition, collapsed across subjects. When the normal and reverse conditions of the same Time X Reference combination are compared to one another with a *two-sided t-test*, no condition reaches statistical significance when corrected for multiple comparisons. When left uncorrected, one condition (150 ms X .125

MC) exceeds a traditional significance of $\alpha = .05$; this is to be expected via random chance. Another test that can be performed is comparing all the *JND* values directly rather than averaging across subjects first. To do this, I used a *paired-sample t-test*, which makes a direct comparison for every Subject X Time X Reference condition in the normal and reversed presentation condition. Once again, I fail to reject the null hypothesis ($p = .40$), further reinforcing the notion that there is no order effect.

Normal Presentation

Display Time	Reference Magnitude (Michelson Contrast)				
	0.05	0.125	0.2	0.275	0.35
300 ms	.014 ± .003	.021 ± .0086	.023 ± .0083	.034 ± .0085	.038 ± .019
150 ms	.015 ± .014	.043 ± .025	.050 ± .035	.051 ± .023	.064 ± .032
125 ms	.056 ± .10	.046 ± .023	.060 ± .028	.045 ± .0099	.090 ± .055
100 ms	.029 ± .015	.059 ± .035	.059 ± .021	.096 ± .034	.11 ± .041
75 ms	.093 ± .033	.059 ± .015	.13 ± .090	.087 ± .044	.15 ± .11
50 ms	.18 ± .08	.11 ± .062	.18 ± .15	.34 ± .40	.19 ± .070

Reversed Presentation

Display Time	Reference Magnitude (Michelson Contrast)				
	0.05	0.125	0.2	0.275	0.35
300 ms	.017 ± .0064	.024 ± .007	.028 ± .0073	.035 ± .0076	.039 ± .0091
150 ms	.024 ± .013	.046 ± .037	.051 ± .027	.055 ± .019	.050 ± .022
125 ms	.047 ± .047	.064 ± .054	.068 ± .026	.075 ± .049	.063 ± .023
100 ms	.053 ± .034	.084 ± .057	.10 ± .058	.13 ± .074	.11 ± .066
75 ms	.079 ± .031	.13 ± .068	.12 ± .051	.14 ± .058	.15 ± .050
50 ms	.17 ± .093	.17 ± .081	.15 ± .064	.19 ± .05	.23 ± .16

Table 3.3: JND results across different conditions

JND data is averaged across subjects and presented for every Time X Reference condition. The top table ('Normal Presentation') contains data from the first half of the experiment, where the reference grating is presented prior to the test grating. The bottom table ('Reversed Presentation') contains data from the second half of the experiment, where the test grating is presented prior to the reference grating. This change occurs without the subject's knowledge. The prompt ('Did the second grating have a higher contrast than the first?') remained unchanged. Note that the 600 ms condition is not presented here, since was only presented in the 'Normal Presentation' condition.

The above analysis leaves open the possibility that, while most people do not have an order preference, occasionally a single subject may have an order preference. To evaluate this possibility, we can look at individual subject JND data, and perform the same *paired-sample t-test* described above. In this, after corrections for multiple comparisons, I found that one subject shows an order effect ($p = .0013$). Since this affected only one

subject, I believe that the counterbalancing that was done (i.e., averaging the results of the normal and reverse presentation conditions) should be sufficient to overcome any problems. However, future studies should be aware of the possibility that individual subjects may have order preferences.

3.3.4 – Fitting stimulus magnitude and duration

In Section 2.2.5, I discussed predictions that the current model makes if we were to analyze it across both display time and reference magnitude using the following equation:

$$(2.44) \quad JND(\tau, \theta) = \alpha_{fit} \cdot (\tau^{-x} \theta^{-y})$$

where τ is the stimulus presentation time (up to τ_{sat}), θ is the reference stimulus magnitude, and $\alpha_{fit} = \alpha_{sat} \cdot \tau_{sat}^{1-\rho}$.

To correctly run the analysis (either analytically or through simulation) and make comparisons to the data, we must find ρ , τ_{sat} and α_{sat} . While I have found that $\rho \cong 0$ and $\tau_{sat} \cong 230 \text{ ms}$ in Section 3.3.1, I have yet to explicitly determine α_{sat} . The value α_{sat} can be derived in one of two ways. If we believe that the stimulus modality in question follows Weber-Fechner's law (see Chapter 1 for a brief overview), then α_{sat} can be determined by calculating the slope of the Reference vs. JND graph at presentation times greater than τ_{sat} . Using standard linear regression, I determined $\alpha_{sat} \cong .071$ ($r^2 = .38$; see Fig 3.6).

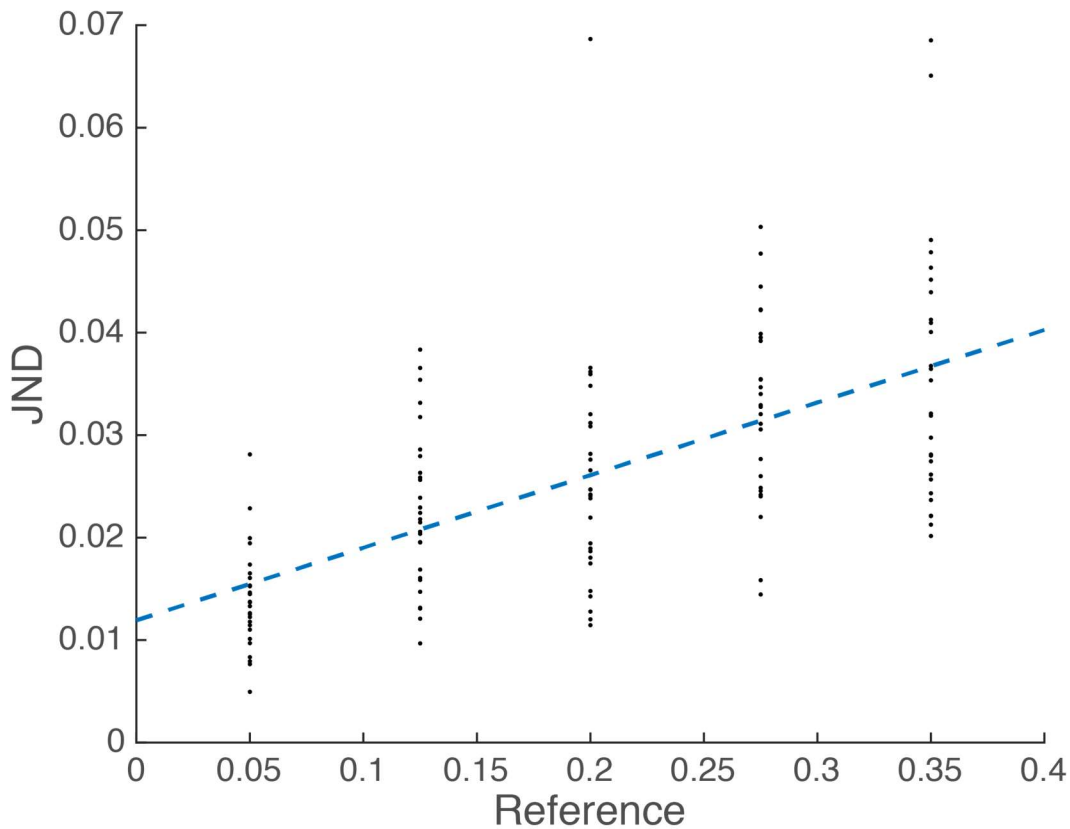


Figure 3.6: Establishing α

Here, I plot the reference intensity against the JND for all subjects for all data recorded above τ_{sat} (i.e., 300 ms and 600 ms conditions). Standard linear regression is used, and α_{sat} is established by measuring the slope ($\alpha_{sat} = .071, r^2 = .38$).

Alternatively, if we were to believe my current data does not follow Weber-Fechner's law, we can fit the same graph to the following equation to calculate a 'correction factor':

$$(2.36) \quad JND = \alpha_{sat} \cdot \theta^{1-\phi}$$

where ϕ is the correction term for sensory modalities that do not perfectly fit Weber-Fechner's law. Note that when $\phi = 0$, Equation 2.36 is exactly Weber-Fechner's law. If the sensory modality is not Weber, ϕ will also be necessary later for predictions in my two-dimensional fit.

By plotting all the reference stimuli vs. the JND and fitting Equation 2.36, it is possible to simultaneously establishing ϕ and α_{sat} . Using the *nlinfit* function in MATLAB, I generated Figure 3.7A and found that $\alpha_{sat} = .17$ and $\phi = .39$. However, this is condensed across display times. It is conceivable that there are large differences for ϕ and α_{sat} across different time conditions. In Figure 3.7B, I separate by times and perform the same fitting procedure. Numerical results are listed below in Table 3.4. While there is variability in α_{sat} and ϕ , when I average for times above τ_{sat} , I find $\alpha_{sat} \cong .056$ and $\phi \cong .54$.

	50 ms	75 ms	100 ms	125 ms	150 ms	300 ms	600 ms
α	.1962	.1879	.2462	.1620	.1010	.0612	.0507
ϕ	.7904	.6192	.2689	.3168	.5346	.5121	.5641

Table 3.4: Numerical results for Weber correction in different time conditions

The above table records the fits of ϕ and α as established fitting the behavioral data to Equation 2.36. The data is broken up into fits for different stimulus display times, corresponding to the different fits shown in Figure 3.7B

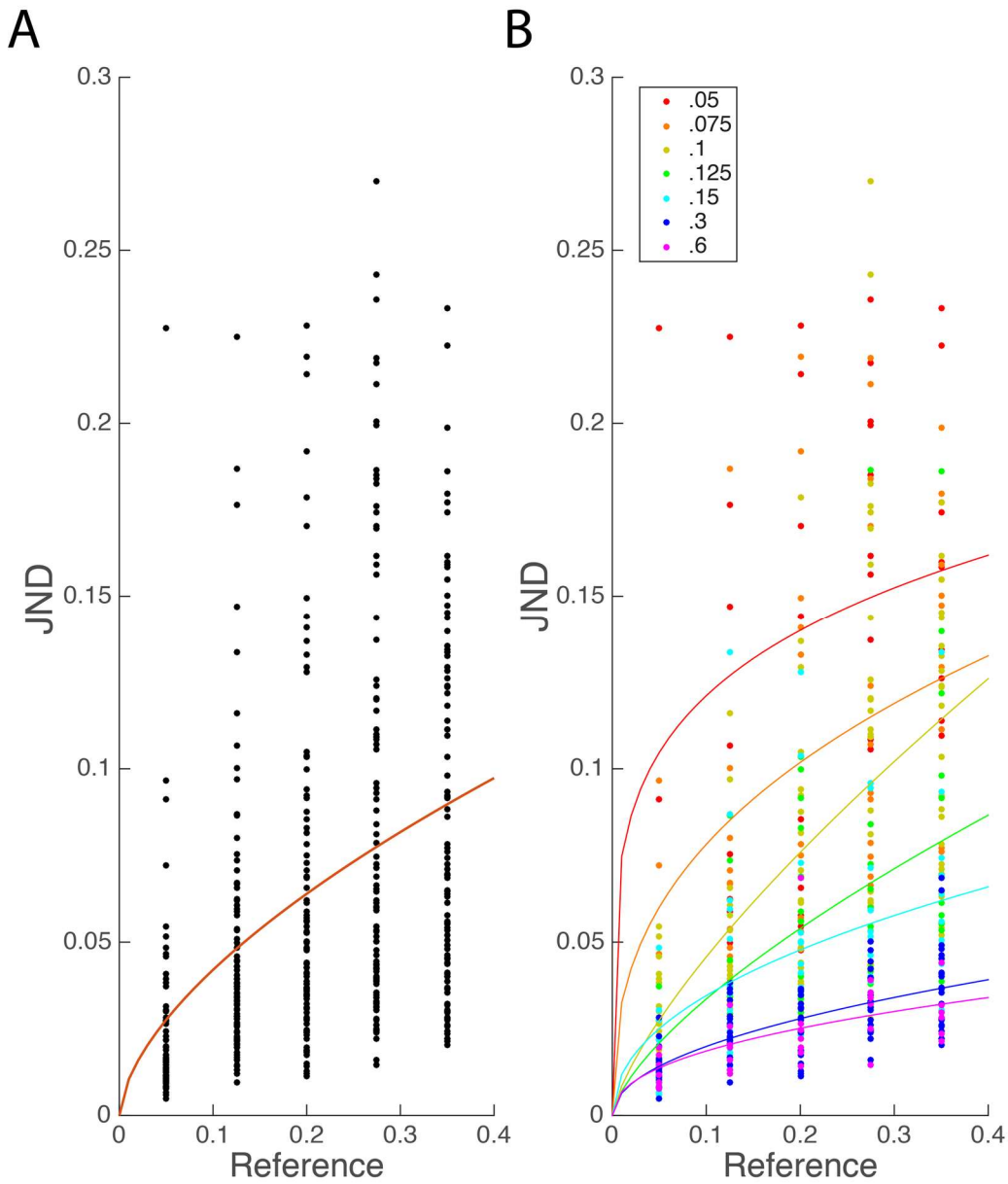


Figure 3.7: Determining ϕ

A: Fitting Equation 2.36 to all the behavioral data ($\phi = .39$). **B:** Fitting the data after separating by stimulus display times. Numerical values for α and ϕ for the different curves are presented in Table 3.4.

With ρ , τ_{sat} , α_{sat} , and (if necessary) ϕ determined, we can determine how well the data fits the two-parameter model described in Equation 2.43. Using the *nlinfit* tool from the MATLAB statistical toolbox, I find that $\alpha_{fit} = .024 \pm .0078$, $x = .83 \pm .11$, and $y = -.47 \pm .11$, with $\pm X$ denoting 95% confidence intervals. This fit, along with the empirical behavioral data, is presented in Figure 3.8.

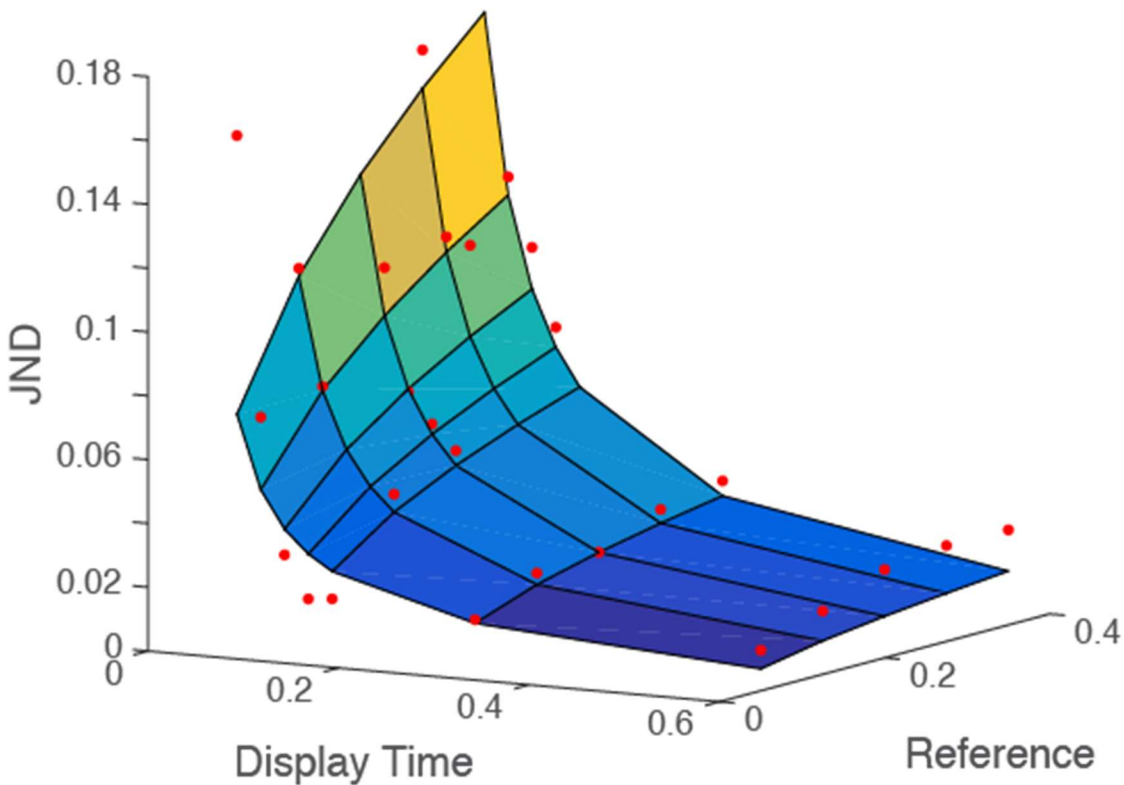


Figure 3.8: Two parameter fitting of the behavioral data

The above 3-Dimensional plot shows the relationship between the reference stimulus magnitude, the display time, and the JND. Behavioral data is shown as red dots. The multicolored plane is a projection of the best fit Equation 2.43 for the behavioral data. Note that at the shortest time (50 ms) and lowest reference magnitude (.05 Michelson contrast), there is an outlier in the data. This is related to the outlier discussed in Figure 3.5, and is not included in the fitting data.

In Section 2.2.5, I showed that different assumptions in my model resulted in different predictions for the parameters α_{fit} , x , and y . I have recapitulated those predictions in Table 3.5. It is important to note that α_{fit} varies from the predictions in the last chapter because I am using a behaviorally determined α_{sat} ; for the Weber cases, I use $\alpha_{sat} = .071$ (as calculated for Figure 3.6), while for Non-Weber cases, I used $\alpha_{sat} = .056$ (as calculated in Figure 3.7). For reference, the conditions being tested are:

- Weber/Poisson: This was my original hypothesis. Poisson noise from neural firing rate stochasticity would influence behavior for a stimulus that followed Weber's law. This would require $\phi = 0$ and a $\rho = .5$.
- Weber/Constant Noise: In this condition, Gaussian noise from some decoder (e.g., memory retrieval, decision, etc.) is used rather than Poisson neuronal noise. This would set $\phi = 0$ and $\rho = 0$.
- Non-Weber/Poisson: Here, noise would come from variability in the spike rate ($\rho = .5$), but it would be for a sensory modality with a Non-Weber stimulus. We would set $\phi = .5$, like what was found for the current data
- Non-Weber/Constant Noise: Finally, I will test for both a non-Weber condition ($\phi = .5$, same as above) and a constant noise condition ($\rho = 0$).

	α_{fit}	x	y	RSS	AICc
Behavior Fit	0.017±.01	0.95±.11	-0.46±12	.011	1
Weber/Poisson	.034	.5	-1	57.86	.18
Weber/Constant	.0163	1	-1	31.06	.25
Non-Weber/ Poisson	.027	.5	-.5	14.49	.37
Non-Weber/ Constant	.013	1	-.5	2.80	.84

Table 3.5: Comparing experimental results to model predictions

In Section 2.6, I derived a model that predicted a double power law relationship (Equation 2.43) between the stimulus magnitude, display time, and JND. Depending on the assumptions the model takes on noise characteristics, as well as whether the stimulus follows the Weber-Fechner law, it changed the expected parameters of the double power law. The assumptions, and their predictions, are listed here. Additionally, I have the parameters determined by the best ‘Fit to Behavior’ (as seen in Figure 3.8) listed at the top. We can compare the goodness of fits of these different models using the Residual Sum of Squares (RSS) and the corrected Akaike Information Criterion (AICc) listed on the right.

To compare these models against one another, I used two techniques (also reported in Table 3.5). The first is a simple Residual Sum of Squares (RSS), which is a useful technique to find the absolute amount of error between the predictions of the model and the behavioral data. The RSS of the model fitted to the experimental results is

tautologically the lowest value. However, the Constant Noise/Non-Weber case comes shockingly close.

To compare these models in a more rigorous way, I also use a technique called the corrected Akaike Information Criterion (AICc). Contrasted to the RSS, the AICc value does not show how good a fit each model is in absolute terms; rather, it shows how good different models are relative to one another. It also adds a complexity cost. In the AICc evaluation, models are penalized for each additional parameter they have. In the case of the 'Fit to Behavioral Results', there is a penalty because it has four free parameters (α_{fit} , x , y , and a Gaussian noise term). In the other models, the values of α_{fit} , x and y are determined, simply leaving the Gaussian noise as the only fit parameter.

Here, the AICc values are all relative to the best fit to behavioral data as found by the *nlinfit* method seen in Figure 3.8. The resulting values can be interpreted like so: 'The Constant Noise/Non-Weber prediction explain the information 84% as well as a least square fit to behavior' (replace the condition and AICc value as appropriate). These results suggest that a tuning curve model with a constant noise and a contrast-scaling exponent (ϕ) of 0.5 can explain the data almost perfectly. Note that this conclusion contradicts my initial hypothesis, namely that the noise controlling the perceptual errors would be close to Poisson.

3.4 - Conclusion

My experimental results show that (1) the noise affecting contrast discrimination is roughly constant and independent of the magnitude of the sensory variable, and that (2) the brain uses a very limited temporal integration window (≈ 230 ms) to form percepts of contrast. The first result contradicts the hypothesis that perceptual errors arise from the variability of the sensory neurons that encode the percept. Below, I discuss how these results compare to previous publications, the theoretical explanations for these results, and the testable ramifications of these theories.

3.4.1 - Behavioral noise

I hypothesized that a likely source for behavioral variability is the trial-by-trial spike count variability (Shouval et al., 2013). My results are inconsistent with this hypothesis since the behaviorally determined ρ value is significantly different ($p \cong .00014$) from the previously determined physiological value of $\rho = 0.58$ for single contrast encoding neurons in V1 (Dean, 1981a). This conclusion remains even if we assume a realistic variable firing rate as described in Section 2.2.3; such an assumption would require the slope of the LJR graph (m) to be $-0.5 \leq m \leq 0$, which is not the case.

A previous experiment also varied the presentation time in a contrast dependent behavioral task (Legge, 1978), but differed from mine in several respects: it used a contrast detection task rather than a discrimination task, a staircase procedure (Wetherill and Levitt, 1965) to estimate the parameters of the psychometric curve rather than Bayesian adaption (Kontsevich and Tyler, 1999), and a smaller number of subjects. I have

approximated the value of ρ from the most comparable portion of that published dataset (i.e., spatial frequency of .75), and found it to be approximately .25. Although this differs from my estimate, due to the difference in the actual experiments I cannot determine what the origin of this difference is, and cannot even determine if it is statistically different from my result.

The value of the ρ that I find in this experiment, as well as that just estimated from previous data (Legge, 1978), is very different than the value one expects from single neurons that encode contrast (Churchland et al., 2010; Dean, 1981a). One possible explanation of this discrepancy is that, since the stimulus is encoded by an ensemble of correlated neurons (and not by a single neuron), some forms of averaging over the population may give rise to a constant noise distribution across the entire ensemble. There is some empirical support for this notion (Chen et al., 2006). However, such an interpretation very puzzling if one assumes that perceptual noise (σ_θ) were to indeed arise from the encoding neurons. Although a combination of correlated Poisson-like neurons could have statistics that differ significantly from Poisson statistics, there seems to be no conceivable way of combining them to obtain a variable in which signal accumulates over time, but noise does not. Therefore, it is highly unlikely that the behavioral errors in contrast perception arise from the variability of the encoding sensory neurons in V1.

An alternative explanation is that the source of perceptual errors arises from a suboptimal decoding process (possibly involving noisy decision or memory operations) with a constant noise level ($\rho = 0$). This suboptimal decoding process would overwhelm any

noise from spike count or timing variability (Johnson, 1980). Such noise added during decoding would be independent of the stimulus duration or contrast. This interpretation is consistent with observations that perceptual errors are far greater than expected from averaging over many sensory neurons (Britten et al., 1993; Tolhurst et al., 1983). However, this alternative seems inconsistent with experiments that report significant choice probabilities in sensory cortical neurons (Britten et al., 1996). One possible explanation is that significant choice probabilities arise from sensory neurons that get top-down feedback from the decoding neurons. In such a case, the behavioral variability does not arise from the variability of the sensory neurons; rather, the decoding process affects the variability of the sensory neurons. Further experiments are needed to resolve this apparent contradiction between my results and previous results regarding choice probabilities of sensory neurons.

To summarize, I have shown that the primary introduction of noise is not in the encoding phase (i.e., stochastic processes translating time and stimulus intensity into firing rates), but rather in the decoding phase (e.g., decision, memory storage and retrieval, comparison). Future experiments should attempt to isolate aspects of the decoding process, and determine which one is the primary contributor to our sensory errors.

3.4.2 - Integration Window

I have found the length of the integration window for discrimination of contrast stimuli to be approximately 232 ms. This is again somewhat similar to Legge (1978) which found τ_{sat} ranging from 50 to 1000 ms, depending on the spatial frequency of the stimuli. For

the spatial frequency closest to my experiment's (.75 cycles/degree of vision), τ_{sat} was found to be approximately 100 ms. While different, as I noted in the above 'Behavioral Noise' section, Legge (1978) used a contrast detection paradigm, where stimuli are determined to be present or absent compared to a blank screen. My study used a discrimination paradigm; similar gratings are displayed, and subjects choose the one with the higher contrast. It may be that detection uses a different mental strategy than discrimination, resulting in the distinct (albeit similar in magnitude) results we see here.

Although the integration window I find is quite short, I propose that it is consistent with established cellular responses to contrast stimuli. It has been shown that contrast-detecting neurons have a highly transient firing rate response whose information content returns to baseline levels after approximately 200 ms (Heller et al., 1995). Given the properties of such sensory neurons, it might not be possible to extract useful information from longer presentation times. While it may be surprising that our visual system is unable to utilize temporal windows longer than 230 ms for contrast perception, it is intriguing to note that this is approximately the same length of time as a standard inter-saccade interval (Carpenter, 1988). I postulate that, if the eyes rarely stay in a single position for longer than ~200 ms, there would be little reason for the brain to be able to integrate over longer time intervals. Both the short inter saccade intervals and integration time window might have arisen because evolutionary pressures favor fast reaction times over very precise stimulus estimation.

Chapter 4: Conclusion

Chapter 4 - Conclusion

The process of perception is prone to systematic errors, and while these systematic errors have been extensively studied, their origin remains a mystery. The goal of this dissertation has been to use a mixture of theoretical and experimental work to show what the physiological basis of sensory errors is – or, failing that, clarify what it is not.

To do this, I started with the hypothesis that neuronal noise was responsible for errors in perception. In Chapter 2, I built a model that showed how spike rate variability could be linked to a behavioral measure of perceptual acuity. Further, I extended upon work done in Shouval et al. (2013) and built a comprehensive neural-like model that could predict the perceptual error rate using stimulus magnitude and duration. In Chapter 3, I developed and implemented a psychophysical experiment that could test the predictions of the work in Chapter 2. The results showed that it was impossible for firing rate variability to account for perceptual errors. At the same time, I verified the neural-like model described above. This model shows that it is possible to construct plausible tuning curves that can explain the effects of stimulus magnitude and duration on perceptual acuity.

In Chapter 2, I focused on building a model based on a series of simple assumptions to link neuronal noise to perceptual errors. The central innovation used was that different statistical distributions for spike counts would be effected differentially by reductions in stimulus duration. This relationship between spiking statistics and behavior was defined analytically, and had the benefit of being easily translatable into a psychophysical

experiment (done later in Chapter 3). This relationship was shown to work regardless of whether the sensory neurons in question had a static or dynamic firing rate.

As a possible alternative to my assumption that perceptual errors originate from the variable spike count of sensory neurons, I considered whether uncertainty of stimulus duration could account for the scaling of perceptual errors as described here. To briefly restate the concern, perceptual judgment is based on the firing rate of the appropriate neurons. To calculate a rate value, time duration must be known. Since it is well established that errors exist in time perception (Buhusi and Meck, 2005; Church, 2003; Gibbon et al., 1984), it is possible that this rate calculation is the origin of perceptual errors for magnitude estimation. I showed that, if timing errors were the primary source of perceptual errors, then it would require there be a nearly constant error rate no matter how long the stimulus duration lasted. This was later shown not to be the case (Chapter 3), suggesting that some other noise source was the origin of perceptual errors.

Finally, I extended the model so that it not only made predictions with respect to how errors depend on stimulus duration, but also how they depend on stimulus magnitude. This was accomplished by further generalizing the model, allowing it to work with sensory modalities that did not perfectly follow Weber-Fechner's law. The analytical work done here resulted in a prediction of a double power law function to explain the relationship between the JND, the stimulus magnitude and its duration. These results were also tested in Chapter 3.

There are several possibilities to extend this analytical work further. One promising theory proposed the idea that uncertainty about the meta-information of a signal (i.e., the information about the information, such as its duration or position of the stimuli) could potentially explain many of the characteristics of perceptual errors that have been discovered (Pelli, 1985). In Chapter 2, I addressed the meta-information of stimulus duration, and showed that it made very specific prediction on the shape of behavioral noise, which turned out to be incompatible with my results (Chapter 3). It would be prudent to look at the other possible types of meta-information uncertainty (e.g., uncertainty on location of the data) and see if a similar functional relationship between this and behavior can be established.

Another possibility for future work is to push the behavioral predictions of my model even further. In nature, stimuli vary in presentation times, sometimes enormously. The current model does not specifically state predictions on what would happen were the reference and test stimuli to have different durations. It is not clear analytically how this would affect perceptual acuity. Further work could establish this, and provide additional feasible test cases.

Finally, the model does not have a method to deal with noise intrinsic to the stimulus, such as occurs in choice probability experiments (Britten et al., 1993, 1996; Shadlen et al., 1996). An interesting phenomenon within these types of experiments is that the

integration time window seems to be substantially longer than for simpler stimuli such as contrast. It is not immediately apparent how introducing noise directly into the stimulus would affect the behavioral predictions of the current model. However, it may be useful to attempt to explain these the results of these noisy stimuli experiments, particularly considering the results from Chapter 3.

In Chapter 3, I applied the work done in Chapter 2 by carrying out a psychophysical experiment. I chose to use contrast stimulus because it satisfied the assumptions in my model, namely that the tuning curve was monotonic (Dean, 1981b) and that the spike count variability was well characterized (Dean, 1981a). To recap the basics of the experiment, varying intensities of gratings were presented to subjects to find their contrast discrimination ability (measured by JND – see Chapter 1 for overview). In order to test the predictions in Chapter 2, the display time of the gratings was manipulated, and the results plotted against Equation 2.2.

Because contrast sensitive neurons have a Poisson spiking variability, I predicted that the slope of the plotted line would be -0.5 . Surprisingly, I found that the slope was approximately -1 , which corresponded to a constant variability, and precludes the possibility that spiking variability is the source of stimulus magnitude estimation errors. In the same analysis, I also discovered that the brain uses a somewhat limited integration time window (approximately 230 ms) to form the percept of contrast.

Finally, I compared the mean contrast discrimination ability across subjects to the neural-like tuning curve model described in Chapter 2. I found that, solely from first principles, it was possible to predict perceptual acuity from stimulus magnitude and duration. Assuming constant noise, and two statistical parameters derived from the data, I can design a tuning curve that will describe the behavior nearly perfectly.

The results here are somewhat surprising. I have shown that, at least with respect to contrast perception, neural variability cannot account for perceptual errors. Rather, whatever physiological mechanism is determining perceptual acuity must have constant noise variability. This likely means that something within the decoding process of the spike train is introducing the noise, possibly memory storage/retrieval (Hubbard, 1994) or decision-making (Johnson, 1980). Another alternative is that, as discussed above, uncertainty regarding the meta-information of a stimulus is causing perceptual errors. While I established analytically that the uncertainty of the meta-information of a stimulus's duration could not account for the current behavioral results, uncertainty of other types of meta-information (e.g., stimulus location) may.

The results regarding the temporal integration window for the perception of contrast are also significant. I found that subjects reach peak performance at approximately 230 ms of presentation time. After this time window, they perform no better regardless of how much time they are given to view the stimuli. This is somewhat in line with previous results (Gorea and Tyler, 1986; Legge, 1978; Schofield and Georgeson, 2000; Watson, 1979),

although it is difficult to compare previous experiments to the current one for methodological reasons.

The most interesting thing about the derived time window here is that it corresponds with two physiological measurements. The first is that neurons show a dynamic response to stimuli; even if a stimulus is presented for extended periods of time, it has been shown that most of the information in neuronal response is found in the first 200 ms of a spike train (Heller et al., 1995). After this, the amount of information with respect to the stimulus drops off precipitously. Second, the inter-saccade-interval (ISI; i.e., the time an eye must wait before it is possible to saccade again) is also approximately 200 ms (Carpenter, 1988). It may be the case that these values are interrelated: from an evolutionary perspective, if your eye does not remain still for longer than 200 ms, there would be no pressure to be able to integrate visual information for longer periods of time, even if it may gain further perceptual accuracy.

The experimental results here suggest many possible future directions. First, I would naturally want to repeat this experiment in different sensory modalities. If saccades play a role in determining the integration window (as hypothesized above), then choosing a modality such as pitch or loudness would help remove the effects of eye movements on sensory processing. Alternatively, I could repeat the current experiment with an eye tracker and see if there is an association between each subject's ISI and their integration window. It also may be possible to 'train' a longer integration window if subjects are given

biofeedback with respect to their eye position and given an incentive to keep their eyes fixed.

Finally, using more complex stimuli would open new avenues of research, and allow us to test the current model in higher order cortical areas. In particular, the results from experiments on 'Choice Probabilities' are extremely relevant to the current line of research (Britten et al., 1993, 1996; Shadlen et al., 1996). This field of psychophysics concerns itself with stimuli that have intrinsic noise. One particular test that they do is having subjects look at moving dots and determine which direction they are moving in; this is complicated by a subset of the dots that are moving in random directions. As stated above, it is not clear how such a stimulus would function within the current model. However, the more interesting fact is that variability in MT neurons has been shown to explain perceptual errors (Britten et al., 1993, 1996; Shadlen et al., 1996). This contradicts the current results, albeit in a different perceptual system and brain region than the one studied here. While I have proposed a possible reason for this (feedback from higher level systems influencing neuronal variability), further experimentation is needed to fully explain this contradiction.

Bibliography

- Albrecht, D.G., Geisler, W.S., Frazor, R.A., and Crane, A.M. (2002). Visual Cortex Neurons of Monkeys and Cats: Temporal Dynamics of the Contrast Response Function. *J. Neurophysiol.* *88*, 888–913.
- Bloch, A.M. (1885). Experiences sur la vision. *CR Seances Soc Biol Paris* 493–495.
- Britten, K.H., Shadlen, M.N., Newsome, W.T., and Movshon, J.A. (1993). Responses of neurons in macaque MT to stochastic motion signals. *Vis. Neurosci.* *10*, 1157–1169.
- Britten, K.H., Newsome, W.T., Shadlen, M.N., Celebrini, S., Movshon, J.A., and others (1996). A relationship between behavioral choice and the visual responses of neurons in macaque MT. *Vis. Neurosci.* *13*, 87–100.
- Buhusi, C.V., and Meck, W.H. (2005). What makes us tick? Functional and neural mechanisms of interval timing. *Nat. Rev. Neurosci.* *6*, 755–765.
- Carpenter, R.H. (1988). *Movements of the eyes* (Ann Arbor (MI): Pion Limited).
- Chen, Y., Geisler, W.S., and Seidemann, E. (2006). Optimal decoding of correlated neural population responses in the primate visual cortex. *Nat. Neurosci.* *9*, 1412–1420.
- Church, R.M. (2003). A concise introduction to scalar timing theory. In *Functional and Neural Mechanisms of Interval Timing*, (Boca Raton, FL, US: CRC Press), pp. 3–22.
- Churchland, M.M., and Abbott, L.F. (2012). Two layers of neural variability. *Nat. Neurosci.* *15*, 1472–1474.
- Churchland, M.M., Yu, B.M., Cunningham, J.P., Sugrue, L.P., Cohen, M.R., Corrado, G.S., Newsome, W.T., Clark, A.M., Hosseini, P., Scott, B.B., et al. (2010). Stimulus onset quenches neural variability: a widespread cortical phenomenon. *Nat. Neurosci.* *13*, 369–378.
- Cohen, M.R., and Newsome, W.T. (2009). Estimates of the Contribution of Single Neurons to Perception Depend on Timescale and Noise Correlation. *J. Neurosci.* *29*, 6635–6648.
- Coren, S., Ward, L.M., and Enns, J.T. (2003). *Sensation and Perception* (Hoboken, NJ: Wiley).
- Dayan, P., and Abbott, L.F. (2005). *Theoretical Neuroscience: Computational and Mathematical Modeling of Neural Systems* (The MIT Press).
- Dean, A.F. (1981a). The variability of discharge of simple cells in the cat striate cortex. *Exp. Brain Res.* *44*, 437–440.
- Dean, A.F. (1981b). The relationship between response amplitude and contrast for cat striate cortical neurones. *J. Physiol.* *318*, 413–427.
- Deco, G., and Rolls, E.T. (2006). Decision-making and Weber’s law: a neurophysiological model. *Eur. J. Neurosci.* *24*, 901–916.

- Deco, G., Scarano, L., and Soto-Faraco, S. (2007). Weber's Law in Decision Making: Integrating Behavioral Data in Humans with a Neurophysiological Model. *J. Neurosci.* 27, 11192–11200.
- Ehrenstein, W.H., and Ehrenstein, A. (1999). Psychophysical Methods. In *Modern Techniques in Neuroscience Research*, P.D.U. Windhorst, and P.D.H. Johansson, eds. (Springer Berlin Heidelberg), pp. 1211–1241.
- Fechner, G.T. (1860). *Elemente der psychophysik* (Leipzig : Breitkopf und Härtel).
- García-Pérez, M.A. (1998). Forced-choice staircases with fixed step sizes: asymptotic and small-sample properties. *Vision Res.* 38, 1861–1881.
- Gescheider, G.A., Bolanowski, S.J., Verrillo, R.T., Arpajian, D.J., and Ryan, T.F. (1990). Vibrotactile intensity discrimination measured by three methods. *J. Acoust. Soc. Am.* 87, 330–338.
- Gibbon, J. (1977). Scalar expectancy theory and Weber's law in animal timing. *Psychol. Rev.* 84, 279–325.
- Gibbon, J., Church, R.M., and Meck, W.H. (1984). Scalar Timing in Memory. *Ann. N. Y. Acad. Sci.* 423, 52–77.
- Gorea, A. (2015). A Refresher of the Original Bloch's Law Paper (Bloch, July 1885). *-Percept.* 6.
- Gorea, A., and Tyler, C.W. (1986). New look at Bloch's law for contrast. *J. Opt. Soc. Am. A* 3, 52–61.
- Goris, R.L.T., Wichmann, F.A., and Henning, G.B. (2009). A neurophysiologically plausible population code model for human contrast discrimination. *J. Vis.* 9.
- Heggelund, P., and Albus, K. (1978). Response variability and orientation discrimination of single cells in striate cortex of cat. *Exp. Brain Res.* 32, 197–211.
- Heinrich, T.S., and Bach, M. (2001). Contrast Adaptation in Human Retina and Cortex. *Invest. Ophthalmol. Vis. Sci.* 42, 2721–2727.
- Heller, J., Hertz, J.A., Kjaer, T.W., and Richmond, B.J. (1995). Information flow and temporal coding in primate pattern vision. *J. Comput. Neurosci.* 2, 175–193.
- Hertz, J., Richmond, B., and Nilsen, K. (2003). Anomalous response variability in a balanced cortical network model. *Neurocomputing* 52–54, 787–792.
- Hubbard, T.L. (1994). Memory psychophysics. *Psychol. Res.* 56, 237–250.
- Indow, T., and Stevens, S.S. (1966). Scaling of saturation and hue. *Percept. Psychophys.* 1, 253–271.
- Johnson, K.O. (1980). Sensory discrimination: decision process. *J. Neurophysiol.* 43, 1771–1792.
- Kandel, E., Schwartz, J., Jessell, T., Siegelbaum, S., and Hudspeth, A.J. (2012). *Principles of Neural Science, Fifth Edition* (McGraw Hill Professional).

- Klein, S.A. (2001). Measuring, estimating, and understanding the psychometric function: A commentary. *Percept. Psychophys.* *63*, 1421–1455.
- Kontsevich, L.L., and Tyler, C.W. (1999). Bayesian adaptive estimation of psychometric slope and threshold. *Vision Res.* *39*, 2729–2737.
- Leek, M.R. (2001). Adaptive procedures in psychophysical research. *Percept. Psychophys.* *63*, 1279–1292.
- Legge, G.E. (1978). Sustained and transient mechanisms in human vision: temporal and spatial properties. *Vision Res.* *18*, 69–81.
- Legge, G.E. (1981). A power law for contrast discrimination. *Vision Res.* *21*, 457–467.
- Mainen, Z.F., and Sejnowski, T.J. (1995). Reliability of spike timing in neocortical neurons. *Science* *268*, 1503–1506.
- May, K.A., and Solomon, J.A. (2015a). Connecting psychophysical performance to neuronal response properties I: Discrimination of suprathreshold stimuli. *J. Vis.* *15*, 8.
- May, K.A., and Solomon, J.A. (2015b). Connecting psychophysical performance to neuronal response properties II: Contrast decoding and detection. *J. Vis.* *15*, 9.
- Mazurek, M.E., Roitman, J.D., Ditterich, J., and Shadlen, M.N. (2003). A Role for Neural Integrators in Perceptual Decision Making. *Cereb. Cortex* *13*, 1257–1269.
- McGill, W.J., and Goldberg, J.P. (1968). A study of the near-miss involving Weber's law and pure-tone intensity discrimination. *Percept. Psychophys.* *4*, 105–109.
- Nieder, A., and Miller, E.K. (2003). Coding of Cognitive Magnitude: Compressed Scaling of Numerical Information in the Primate Prefrontal Cortex. *Neuron* *37*, 149–157.
- Paradiso, M.A. (1988). A theory for the use of visual orientation information which exploits the columnar structure of striate cortex. *Biol. Cybern.* *58*, 35–49.
- Pelli, D.G. (1985). Uncertainty explains many aspects of visual contrast detection and discrimination. *J. Opt. Soc. Am. A* *2*, 1508–1532.
- Schofield, A.J., and Georgeson, M.A. (2000). The temporal properties of first- and second-order vision. *Vision Res.* *40*, 2475–2487.
- Seung, H.S., and Sompolinsky, H. (1993). Simple models for reading neuronal population codes. *Proc. Natl. Acad. Sci. U. S. A.* *90*, 10749–10753.
- Shadlen, M.N., Britten, K.H., Newsome, W.T., and Movshon, J.A. (1996). A computational analysis of the relationship between neuronal and behavioral responses to visual motion. *J. Neurosci.* *16*, 1486–1510.
- Shouval, H.Z., Agarwal, A., and Gavornik, J.P. (2013). Scaling of Perceptual Errors Can Predict the Shape of Neural Tuning Curves. *Phys. Rev. Lett.* *110*, 168102.

Snowden, R., Thompson, P., and Troscianko, T. (2012). *Basic Vision: An Introduction to Visual Perception* (Oxford: Oxford University Press).

Stein, R.B., Gossen, E.R., and Jones, K.E. (2005). Neuronal variability: noise or part of the signal? *Nat. Rev. Neurosci.* *6*, 389–397.

Stevens, S.S. (1961). To Honor Fechner and Repeal His Law: A power function, not a log function, describes the operating characteristic of a sensory system. *Science* *133*, 80–86.

Tolhurst, D.J., Movshon, J.A., and Thompson, I.D. (1981). The dependence of response amplitude and variance of cat visual cortical neurones on stimulus contrast. *Exp. Brain Res.* *41*, 414–419.

Tolhurst, D.J., Movshon, J.A., and Dean, A.F. (1983). The statistical reliability of signals in single neurons in cat and monkey visual cortex. *Vision Res.* *23*, 775–785.

van Vreeswijk, C., and Sompolinsky, H. (1996). Chaos in neuronal networks with balanced excitatory and inhibitory activity. *Science* *274*, 1724.

Watson, A.B. (1979). Probability summation over time. *Vision Res.* *19*, 515–522.

Weber, E.H. (1834). *De Pulsu, resorptione, auditu et tactu. Annotationes anatomicae et physiologicae ...* (Lipsiae Leipzig: C.F. Koehler).

Wetherill, G.B., and Levitt, H. (1965). Sequential estimation of points on a psychometric function. *Br. J. Math. Stat. Psychol.* *18*, 1–10.

Wijsman, R.A. (1973). On the Attainment of the Cramer-Rao Lower Bound. *Ann. Stat.* *1*, 538–542.

Zhong, Q., Roychowdhury, V.P., Boykin, P.O., and Nirenberg, S. (2005). Non-Poisson Fluctuation Statistics In Neuronal Inter-Spike Intervals (ISI): Hurst parameter Estimates of Mouse Retinal Ganglion Signals. In *2005 IEEE Engineering in Medicine and Biology 27th Annual Conference*, pp. 2095–2098.

Vita

Jonathan Flynn was born in Raleigh, North Carolina on October 2, 1987, the son of Kathryn and Richard Flynn. After completing his work at Chapel Hill High School, Chapel Hill, NC in 2005, he entered the University of North Carolina at Wilmington. He received a Bachelor of Science in Physics, a Bachelor of Arts in Psychology, and a Bachelor of Arts in Philosophy in May, 2010. In August of 2010, he entered the University of Texas MD Anderson Cancer Center UTHealth McGovern Graduate School of Biomedical Sciences.

Permanent address:

1902 S Hgwy 15-501

Chapel Hill, NC 27517